UNIVERSITY OF CALIFORNIA SAN DIEGO

Screening, isolation and characterization of *Brachypodium distachyon* mutants in stomatal CO_2 signal transduction

A Thesis submitted in partial satisfaction of the requirements for the degree of Master of Science

in

Biology

By

Felipe Jesus Rangel

Committee in Charge:

Professor Julian Schroeder, Chair

Professor Alisa Huffaker

Professor Martin Yanofski

2020

The Master's Thesis of Felipe Jesus Rangel is approved, and it is acceptable in quality and form for publication on microfilm and electronically:

Chair

University of California San Diego

2020

DEDICATION

I dedicate this to all my friends and family. Without their support, I would not have been able to achieve the level of growth I have today. A seugirle echándole ganas!

EPIGRAPH

When things go wrong as they sometimes will, when the road you're trudging seems all uphill, when the funds are low and the debts are high, and you want to smile but you have to sigh…Rest if you must, but don't you quit…Success is failure inside out… and you can never tell how close you are, it may be near when it seems so far, so stick to the fight when you're hardest hit-it's when things seem the worst that you must not quit

-John Whittier Greenleaf

TABLE OF CONTENTS

LIST OF FIGURES

LIST OF TABLES

Acknowledgements

I would like to acknowledge Dr. Paulo H.O. Ceciliato, Morgana Sidhom, and Bryn Lopez for their hard work and dedication to the Brachy team. Thank you, Paulo, for being a phenomenal mentor and helping me lay a strong foundation as a scientist. Without your guidance, I would not be the scientists I am now. Obrigado Paulo!

ABSTRACT OF THE THESIS

Screening, isolation and characterization of *Brachypodium distachyon* mutants in stomatal CO_2 signal transduction

by

Felipe Jesus Rangel

Master of Science in Biology

University of California San Diego, 2020

Professor Julian Schroeder, Chair

Plants have evolutionarily developed mechanisms that enable them to adapt and respond to environmental stimuli, increasing plant survivability. A key component involved in these mechanisms are stomatal pores that regulate gas exchange. Stomatal pores are in charge of regulating the intake of CO_2, which is used during photosynthesis to create energy, while

releasing oxygen that humans and animals breathe and minimizing the amount of water loss via evapotranspiration. Plant water loss reduces leaf temperature and can be used as a tool to measure plant transpiration. In monocot grasses, stomatal pores are made up of two dumbbell-shaped guard cells and flanked by two subsidiary cells. These specialized subsidiary cells have been shown to play an important role in promoting faster stomatal opening and closing to stimuli like CO_2. So far, very little is known about the different molecular elements involved in the CO_2 sensing and response mechanisms in grasses. Therefore, to identify potential novel components involved in CO_2-dependent stomatal movement, infrared thermal imaging was utilized in a forward genetic screen using EMS mutagenized plant lines from the grass model *Brachypodium distachyon*

Stomatal pores are found on the abaxial(lower) and adaxial(upper) side of leaves. Changes to the patterning or development of stomatal pores on leaves affects the overall gas exchange. The elements involved in stomatal development and patterning are well understood in the dicot, *Arabidopsis thaliana*. It has been shown that pro-peptide signals known as EPIDERMAL PATTERNING FACTORs (EPFs) regulate stomatal development. Moreover, it has been shown that some subtilase proteases from the (SBT) family can cleave EPF peptides. Cleaved EPFs in turn become activated EPF peptide signals, inducing stomatal regulation. The function of SBT proteases in the monocot, *Brachypodium distachyon* has not been investigated. Therefore, a reverse genetic screen was conducted as a pilot study using artificial microRNA technology to investigate if downregulating selected family members of the SBT family would affect stomatal development in the grass model

General Introduction:

Stomatal pores on the surface of leaves have helped plants sense and adapt to changes in their local and diverse global environments (Hetherington & Woodward, 2003), allowing plants to survive during stressful conditions. Stomatal pores regulate the intake of CO_2 while reducing the loss of water. Therefore, this regulation affects plant photosynthesis (Brodribb et al., 2019) transpiration and, ultimately, plant growth and development. In the dicot plant model *Arabidopsis thaliana*, stomatal pores are made up of a central pore with two surrounding kidney-shaped guard cells. These guard cells influence stomatal pore opening and closing by integrating environmental stimuli and then changing their turgidity (McAinsh & Taylor, 2016). Reduction in guard cell turgidity leads to stomatal pores opening and an increase in guard cell turgidity leads to stomatal closing (Assmann & Jegla, 2016; Munemasa et al., 2015). Some examples of environmental stimuli that induce stomatal closure are high CO2, darkness, pathogen-associated molecular pattern molecules (PAMPs) and drought. Meanwhile, humidity, low CO_2 and red and blue light induce stomatal opening. Stomatal pores protect plants from drying during droughts (Vahisalu et al., 2008) by recognizing the drought hormone known as abscisic acid (ABA) (Munemasa et al., 2015). The recognition of ABA leads to induced stomatal closure and reduction of guard cell turgidity by activating a guard cell expressed anion channel, SLAC1, (Negi et al., 2008; Pei et al., 1997; Vahisalu et al., 2008) leading to the efflux of solutes and a change in membrane polarity causing release of water.

In the grass model *Brachypodium distachyon,* stomatal structure differs from *Arabidopsis thaliana*. The stomatal structure of grasses is made up of two dumbbell shaped guard cells and

two flanking subsidiary cells (McKown & Bergmann, 2020). Very little is known about how subsidiary cells function, but they are thought to be ion sinks that increase stomatal opening and closing (Cai et al., 2017). *Brachypodium distachyon* is phylogenetically related to wheat, barley and shares similar stomatal pore structure with many food crops making it a useful plant model (Brkljacic et al., 2011).

CO_2 and ABA have been shown to share molecular components in their signaling pathways to induce stomatal movements. CO_2 first enters plant cells through proteins known as aquaporins, which facilitate the transport of small molecules, and is perceived after its conversion into bicarbonate (HCO_3^-) by carbonic anhydrases (BETA CARBONIC ANHYDRASE 1 and BETA CARBONIC ANHYDRASE 4) (Hu et al., 2010; J. Zhang et al., 2018). The CO_2 converted bicarbonate can interact with the guard cell expressed anion channel, SLAC1, inducing stomatal closure(J. Zhang et al., 2018). Plants with impairments in the CO_2 signaling pathway have been observed to show differences in leaf temperature(Hashimoto et al., 2006). Further research is required to better understand the different elements involved in CO_2-dependent stomatal opening and closing.

Since the industrial revolution, the level of atmospheric CO_2 has increased rapidly (Scripps Institution of Oceanography, 2018). Brachypodium is a great plant model to investigate the different elements involved in the CO_2 signaling pathway as it is phylogenetically related to monocot species used as food crops (Brkljacic et al., 2011) and can aid in predicting how plants will adapt to their changing environment. With additional research on the CO_2 signaling pathway, the knowledge at hand could in the future help crop bioengineers generate climate-proof crops that survive and show improved yield and water-use efficiency

Chapter 1: Exploiting Canopy Leaf Temperature to Identify Mutants Impaired in Stomatal Movements

1.1 Introduction:

The rise in atmospheric CO_2 and other greenhouse gases over the last century is causing a sense of urgency to understand the mechanisms associated with plant growth (Reddy et al.,

2010). Plants have evolved mechanisms that allow them to regulate photosynthesis and water loss as new leaves grow (Zoulias et al., 2018). Microscopic pores in the epidermis of leaves, known as stomata, play a key role in these processes that help plants sense and respond to different environmental stimuli. They are responsible for maximizing the uptake of CO_2 used for photosynthesis while minimizing water loss.

The stomata of most plant species consist of two kidney-shaped guard cells, meanwhile the stomatal complex of grass species contains two dumbbell-shaped guard cells and two subsidiary cells (Cai et al., 2017). Subsidiary cells are interesting because they have been linked to improving stomatal opening and closing (Raissig et al., 2017). Water loss in plants affects overall water-use efficiency and since grasses provide the vast majority of human calories (Brkljacic et al., 2011) it is of great interest to understand the regulation of the stomatal complexes for future crop engineering

Guard cells regulate the aperture of stomatal pores (Engineer et al., 2016). When guard cell turgidity increases, stomatal opening is induced, whereas a decrease in guard cell turgidity leads to stomatal pore closing. Guard cells respond to various environmental signals such as light, CO_2, and drought by producing a change to pore size (McAinsh & Taylor, 2016). Moreover, exposure to pathogen-associated molecular patterns (PAMPs) also impact stomatal opening and closing via different signaling mechanisms.

Stomatal pores play a key role in plant development. They regulate the flux of gases such as CO_2, O_2, and loss of water via transpiration. The loss of water functions as a way for plants to cool off internally, which in turn lowers the canopy leaf temperature. Therefore, leaf temperature can be used to identify mutants with impaired stomatal control (Negi, Hashimoto-Sugimoto, Kusumi, & Iba, 2014). There have been various mutants published that show a difference in

canopy leaf temperature due to impairments in signaling components involved in stomatal opening and closing. The first *Arabidopsis thaliana* mutant isolated using leaf temperature as an indication of impairments of stomatal responses is the *ht1* (*high leaf temperature 1*) mutant (Hashimoto et al., 2006). The *ht1* mutant shows a warmer leaf temperature relative to wild-type control due to impaired stomatal opening response (Hashimoto et al., 2006; Nordtrom-Israelsson et al. 2015). Moreover, *Arabidopsis thaliana* double-mutant plant in the β-carbonic anhydrases βCA1 and βCA4 show a slower CO_2-dependent stomata response, but respond normally to the hormone abscisic acid and blue light (Hu et al., 2010).

It has been shown that β-carbonic anhydrases (βCA1 and βCA4) function in CO_2-regulated stomatal responses by converting CO_2 into bicarbonate (HCO_3^-). Data indicate that intracellular bicarbonate is responsible for transducing the CO_2 signal that leads to stomatal closure (Xue et al., 2011; J. Zhang et al., 2018). Specifically, bicarbonate has been shown to bind to and activate an anion channel found in guard cells, SLAC-1, which releases solutes to influence guard cell turgidity (J. Zhang et al., 2018).

Using thermography, (Kusumi et al., 2012) scientists were able to isolate a SLAC1-deficient mutant in rice using reverse genetics, that shows a constitutive cool leaf temperature. The reason for this phenotype is that the lack of SLAC1 leads to an increase in stomatal conductance (Negi, Hashimoto-Sugimoto, Kusumi, & Iba, 2014). Understanding that guard cells respond to different stimuli such as light, drought and CO_2 by opening or closing stomata, thermal imaging can be used to identify mutants with stomatal movement impairments with respect to a specific stimulus. For example, the *ost1* mutants were identified in a genetic screen using thermal imaging on drought-stressed plants(Merlot et al., 2002), and showed a lower leaf temperature compared to wild-type (Hashimoto et al., 2006). OPEN STOMATA1 (OST1),

encodes a protein kinase important for stomatal response ABA signaling (Mustilli et al., 2002), that activates the SLAC1 anion channel by phosphorylation (Brandt et al., 2012; Geiger et al., 2009; Lee et al., 2009).

Using thermography to screen mutants in *Arabidopsis thaliana* for impairments in stomatal movements has been successful. However, so far there is no published research on screening for impairments in stomatal movements in grasses. In our forward genetic screen, we used an Ethyl methanesulfonate (EMS) mutagenized population to identify putative mutants with impairments in stomatal movements. We have been able to identify 21 putative mutants that show a difference in canopy leaf temperature relative to wild-type, Bd21-3, at ambient CO_2. These mutants may help give us an insight on the different elements involved in CO_2-dependent stomatal movement signaling and potentially help translate into generating crop plants with faster stomatal movements. As a result, plants would have improved water-use efficiency, and, potentially overall, improved performance under limited water conditions.

1.2 Results:

1.2.1 Forward Genetic Screen for stomatal movement responses in the grass model, *Brachypodium distachyon*

Epidermal pores in leaves, known as stomata, play a key role in plant development. They allow the intake of CO_2 used to produce chemical energy via photosynthesis, while minimizing water loss. Therefore, understanding the different elements that regulate the opening and closing of stomata can be of great interest for increasing carbon uptake, improving water-use efficiency and, overall, plant fitness. Since stomatal pores impact transpiration, leaf temperature can be used as a proxy to identify mutants with impairments in stomatal movements. In our forward genetic screen, a thermal imaging camera was used to identify putative mutants with altered canopy leaf temperature relative to our WT, Bd21-3, control at ambient CO_2.

Brachypodium distachyon is a grass model that is phylogenetically related to wheat and barley and it's diploid genome makes it the simplest genome described in grasses to date (Draper et al., 2001). Compared with rice, *B. distachyon* has a more rapid life cycle, and a smaller stature, (Draper et al., 2001) making it very easy to conduct enhanced-throughput experiments. We conducted a forward genetic screen using a library of over 1,000 EMS mutagenized M5 generation *Brachypodium distachyon* plant lines. Before the initial screen was conducted, Dr. Paulo H.O. Ceciliato first conducted pilot experiments to determine the best approach of screening the mutant lines. The EMS mutagenized plant lines were exposed to high or low CO_2 for 3 hours and then imaged. This process rendered the *chill*1 mutant but was found to be ineffective due to the limited space of growth chambers and the great amount of time it took to screen. In order to optimize Dr. Paulo H.O. Ceciliato's pilot experiments, I helped implement improvements over two years to increase screening efficiency and conserve the ability to identify robust mutants. The first improvement was to stop exposing plants to either high or low CO_2 for 3 hours and then conducting thermal imaging. Rather, we decided to image plants at ambient CO_2, where the plants were grown. This not only cut down the time it took to screen rounds, but

we were able to generate a system where we could grow staggered batches that would allow us to increase the amount of plant lines screened per week. (Note that we are now using high CO_2 exposure for bulk segregant analyses of F2 mutant population). Moreover, in our initial screen, plants were grown in Medium-sized pots. The time-consuming process of preparing pots for all plants prevented us from preparing multiple rounds at a time. As a result, we decided to use smaller sized pots in order to use less amounts of soil while increasing the amount of plant lines in each round. This allowed us to go from 30 plant lines per round to 45, with an overall decrease in amount of work needed to prepare screening rounds. This increase in throughput allowed us to screen and identify putative mutants quickly and efficiently. Lastly, within the initial screen, all plants were staked once they were 2-3 weeks old in order to grow tall-healthy plants and get good quality images. In order to do that, we increased the light intensity from an average of 100 umol. $m^{-2}s^{1}$ to 250 umol. $m^{-2}s^{1}$. In addition, we improved the soil mixture by adding a ratio of vermiculite and perlite to increase the soil's ability to retain moisture. Improving our growth conditions promoted healthier growth of plants that could stand tall on their own, give us good quality thermal images meanwhile circumventing one more unnecessary step.

1305 individual plant lines were screened by growing and imaging rounds of 45 plant lines with 5 biological replicates in the M5 generation (Figure 1.1). EMS-driven mutagenized plant lines and WT control, Bd21-3 were grown to 4-5 weeks before conducting thermal imaging. WT control and mutant plants were grown in parallel and imaged next to each other on top of a cart in the growth room where they are grown. Initially, we identified 50 plants lines that showed either a cooler or warmer canopy leaf temperature relative to the WT control at ambient CO_2. To test reproducibility, each plant line that showed a warmer or cooler leaf temperature relative to the WT control at ambient CO_2 was imaged a week afterwards to confirm leaf temperature

phenotype. Next, in a secondary screen the 50 plants lines in the M5 generation were regrown from our 1305 M5 seed stock and reimaged. After reimaging the regrown M5 generation, 28 out of the 50 plant lines showed consistent canopy leaf temperature phenotypes observed in the primary screen. To characterize the phenotype of the confirmed lines, M5 generation seeds were selected and the M6 generation was grown and stomatal development analysis, thermal imaging after exposure to high CO_2 and gas exchange analyses was conducted. 12 of the 28 plant lines were confirmed in the M6 generation as showing reproduced cooler leaf temperatures (*chill* 1, 2, 3, 4, 5, 6, 10, 11, 12, 13, 14, 15, 16). Some of the first putative mutants to be confirmed in the M6 generation were *Chill 2, 3, 4* (Figure 1.2).

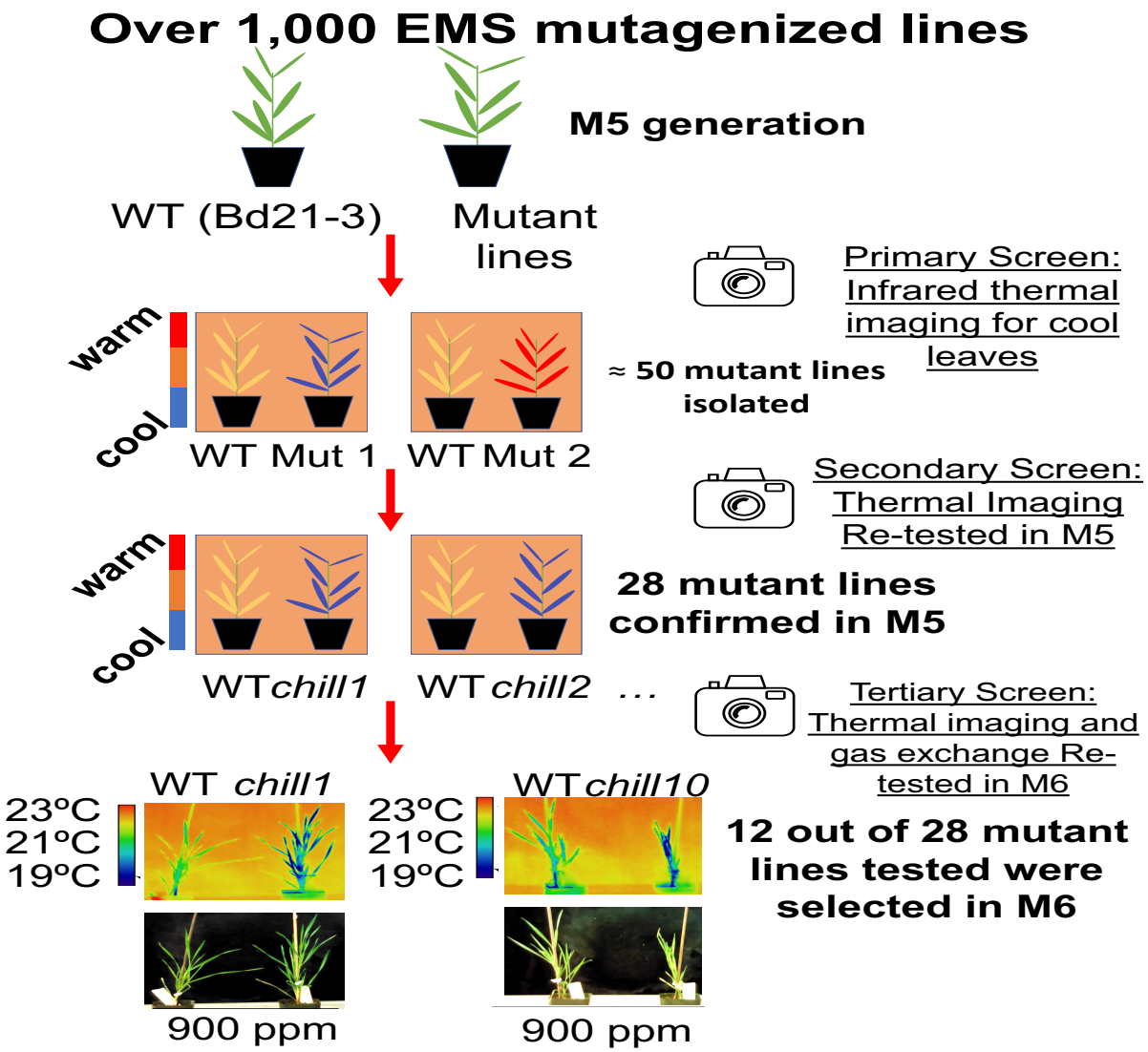

Figure 1.1: Forward Genetic Screen for stomatal movements in grass model. An EMS mutagenized *Brachypodium distachyon* library of over 1000 M5 generation lines were screened for impairments in stomatal movements. Wild-type, Bd21-3, and mutant plants were grown to 5 weeks and imaging was conducted at ambient CO_2 (400ppm) using a thermal camera. The enhanced throughput screen consisted of growing rounds that tested about 45 mutant lines in the M5 generation each round. Each mutant line and Bd21-3 had 5 biological replicates per round. We initially identified 50 mutant lines that showed either a warmer or cooler leaf temperature relative to the wild-type control at ambient CO_2. In a secondary screen, we retested these 50 lines by regrowing the M5 generation and imaging them at ambient CO_2 to determine if the leaf temperature phenotype would reappear. After retesting the 50 lines, only 28 lines maintained the phenotype seen previously. These 28 lines were tested in a tertiary screen in the M6 generation by imaging them after exposure to high CO_2 (900ppm) for 3 hours and gas exchange analyses.

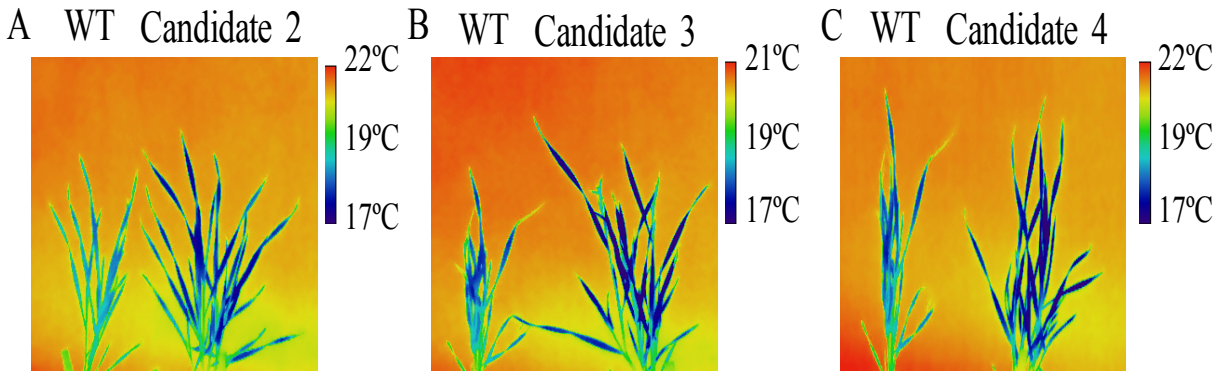

Figure 1.2: Thermal Imaging of M6 generation *chill* mutants at ambient CO_2, where *chill* 2, 3 & 4 were analyzed. Shown are thermal images of the *chill 2*, 3, and 4 mutant at ambient CO_2. (A,B,C). Bd21-3 and every respective *chill* mutant were grown in parallel. All plants were grown under the same conditions. The plants were grown under 16/8 light/dark cycle and the light intensity the plants were exposed to was, on average, 300 umol $m^{-2}s^{-1}$.

1.2.2 *Characterization of the 21 putative chill mutant lines*

Mutants with impairments in stomatal movements have been shown to exhibit a difference in canopy leaf temperature relative to the WT control (Hashimoto et al., 2006). Environmental signals like ABA, CO_2, and light, regulate stomatal movements. Characterization of 21 of the 28 putative mutants in the M6 generation was conducted to gain insight into the stomatal development and response to CO_2-shifts of the putative mutants. Note that 7 of the original 28 M5 mutants were not confirmed during initial experiments of thermal imaging in the M6 generation and therefore are not included in Table 1.1, showing 21 of the original 28 mutants. In

order to determine whether the cool leaf temperature could be reproduced in the next generation, thermal imaging at ambient CO_2 was conducted in the M6 generation. In (Figure 1.2 A) we see thermal imaging of 5-week-old *chill* 2 next to WT control, Bd21-3, at ambient CO_2. *Chill*2 shows a clear cooler leaf temperature relative to the WT control, but also seems to be larger than the WT control. In (Figure 1.2. B) we see a thermal image of 5-week-old *chill*3 and Bd21-3 together at ambient CO_2. *Chill*3 shows a cooler leaf temperature relative to the WT control, Bd21-3, but it is a less clear phenotype than *chill* 2 at ambient CO_2. Lastly, in (Figure 1.2.C.) 5-week-old *chill*4 was thermally imaged next to Bd21-3 at ambient CO_2. *Chill*4 shows a cooler leaf temperature relative to Bd21-3 while also being the same height as the control.

To continue characterizing the 21 mutant plants in the M6 generation, we tested their response to high CO_2. High CO_2 induces stomatal closure in plants, which leads to an increase in leaf temperature. Exposing the *chill* mutants to high CO_2 allowed us to determine if some mutants were insensitive to high CO_2 by maintaining cooler leaf temperature relative to WT controls. *Chill* 1, 2, 3, 4, 5, 10, 15, 16 all showed a cooler leaf temperature relative to the WT control, whereas the rest of the plants *chill* 6, 7, 8, 9, 11, 12, 13, 14, 18, 19 showed a similar canopy leaf temperature as WT, Bd21-3.

Next, in order to determine whether stomatal development played a role in the leaf temperature phenotypes found in the putative mutants, stomatal imaging was conducted on 5-6-week-old plants. The 4^{th} true leaf would be excized and using an epidermal peel technique developed by Morgana Sidhom and I, stomatal imaging was conducted using a DIC microscope. Stomatal density and index were calculated, and our results showed all *chill* mutants having WT-like stomatal development. In addition, using the stomatal images taken to analyze stomatal development, stomatal morphology of the mutants was observed to highlight potential

differences between the WT control and *chill* mutants. All *chill* mutants had similar stomatal morphology as WT, in that they contained 2 dumbbell shaped guard cells and 2 flanking subsidiary cells.

To further characterize the 21 *chill* mutants, gas exchange analyses were conducted to measure stomatal conductance in response to [CO_2] shifts. Healthy 5 to 6-week-old plants were used to conduct gas exchange analysis and were first equilibrated to 400ppm for 1 hour before data recording began. Once the plants equilibrate, plants are first exposed to CO_2 (400ppm) for 30 minutes, then 90 minutes of low CO_2 (150ppm) and lastly high CO_2 (900ppm) for 1 hour. Our results indicate that *chill* 1 and 15 have impaired responses to high CO_2-induced stomatal closure, whereas *chill* 10 is partially impaired (table 1.1). With the gas exchange analysis data, 6 groups were made to separate the mutants based on their response to [CO_2] shifts. Group 1- Mutants with impaired responses to [CO_2] shifts in gas exchange analyses: candidates1, 10, and 15 (and potentially 11, 12). Group 2 - Mutants with distinct kinetics of stomatal responses to [CO_2] shifts: candidates 11, 12 and potentially 21. Group 3 - Mutants with lower steady-state stomatal conductance compared to WT: candidates 3, 11 and 12. Group 4 - Mutants with higher steady-state stomatal conductance compared to WT: candidates 6, 9, 14, 17, 19 and potentially 8. Group 5 - Mutants that show potential stomatal re-opening at high [CO_2]: candidates 2, 9, 13 and perhaps 5. Group 6 - Mutants presenting largely WT-like responses to [CO_2] shifts: candidates 2, 4, 7 and 16.

Table 1.1: Characterization of the 21 putative *chill* mutants. Shown is a table characterizing all *chill* mutants. The table is a compilation of all the data obtained from thermal imaging, stomatal imaging and LiCOR gas exchange analysis. In total, 12 of 21 mutants listed above were confirmed in the thermal imaging screening of the M6 generation plants and the remaining *chill* 20 line of the 28 putative mutants will be analyzed. (Seven of the original 28 M5 mutants were not confirmed during initial experiments of thermal imaging in the M6 generation and therefore are not included in the table showing 21 of the original 28 mutants.

Re-tested candidates in M5 generation: Colder than Wild Type at Ambient CO2	Confirmed in M6 generation ?x=confirmed No=not confirmed	Stomatal Density Imaging X=done	Results on Stomatal Density	High CO2 (900ppm) Thermal Imaging in M6 generation X=done	Results of Thermal imaging under high CO2	LiCOR Gas Exchange (CO2) X=done	Insensitive to CO2	LiCOR Gas Exchange (ABA) X=done	Whole Genome Seq.
chill1	x	x	WT-like	x	colder	x	yes	x	x,x**
R6-33 (*chill2*)	x	x	WT-like	x	colder	x	no	NA	x
R4-45 (*chill3*)	x	x	WT-like	x	colder	x	no	NA	x
R5-18 (*chill4*)	x	x	WT-like	x	colder	x	no	NA	x
R6-18 (*chill5*)	x	x	WT-like	x	colder	x	no	NA	x
R21-29 (*chill6*)	No	x	WT-like	x	WT-like	x	Gs shifted slightly up	NA	
R21-32 (*chill7*)	No	x	WT-like	x	WT-like	x	no	NA	
R21-30 (*chill8*)	No	x	WT-like	x	WT-like	x	no	NA	
R21-33 (*chill9*)	No	x	WT-like	x	WT-like	x	gs shifted up	NA	
R20-7 (*chill10*)	x	x	WT-like	x	colder	x	partial	ongoing	x**
R20-8 (*chill11*)	x	x	WT-like	x	WT-like	x	less low CO2 sens.	NA	
R20-18 (*chill12*)	x	x	WT-like	x	WT-like	x	Unusual CO2 gs	NA	x**
R20-38 (*chill13*)	x	x	WT-like	x	WT-like	x	no	NA	x,x**
R20-40 (*chill14*)	x	x	WT-like	x	WT-like	x	gs shift slightly up	NA	x
R20-41 (*chill15*)	x	x	WT-like	x	colder	x	yes	x	x,x**
R20-43 (*chill16*)	x	x	WT-like	x	colder	x	no	NA	x
R30-4 (*chill17*)	No	NA	NA	NA	NA	x	gs shifted up	NA	x**
R31-1 (*chill18*)	No	NA	NA	x	WT-like	x	gs shifted up	NA	
R31-34 (*chill19*)	No	NA	NA	x	WT-like	x	gs shifted up	NA	x**
R31-7 (*chill20*)	Growing								x**
R30-5 (*chill21*)	No	NA	NA	NA	NA	x	gs shifted up	NA	x**

1.2.3 *Identifying the Causative mutation:*

To identify the causative mutation in the *chill* mutants, two approaches were taken. The mutants confirmed in the M6 generation were sent for initial whole genome sequencing and in parallel, *chill* 1, 10 and 15 were backcrossed with the parental line, Bd21-3, to generate an F2 mapping population (Figure 1.7). To determine whether the causative mutation was dominant or recessive, phenotypic assays were conducted on the F1 backcrosses. The F1 backcrosses were exposed to high CO_2 along with the mother plants and were thermally imaged afterwards (Figure 1.3.A, & 1.5.A). In (Figure 1.3.A.), Bd21-3, *Chill*1 and Bd21-3 x *chill* 1 backcross are thermally imaged after exposure to high CO_2. *Chill*1 shows a cooler leaf temperature relative to WT, Bd21-

3, whereas the *chill*1 backcross shows a canopy leaf temperature similar to WT, Bd21-3. In addition, in (Figure 1.3.A.) all plants are similar in size, and the soil moisture in all three pots is similar. Further gas exchange analysis experiments were conducted on the Bd21-3 x *chill* 1 F1-generation backcross to determine whether the causative mutation was dominant or recessive. In (Figure 1.3.B) we see stomatal conductance measurements of *chill*1 and WT, Bd21-3. At 400 ppm, *chill* 1 has similar stomatal conductance as WT and when exposed to low CO_2 (150ppm) *chill*1 responds like WT with an increase in stomatal conductance. Moreover, when exposed to high CO_2 (900ppm), *chill*1 does not show a decrease in stomatal conductance as seen for WT.

Furthermore, in (Figure 1.3.C) gas exchange analysis of WT and F1-generation Bd21-3 x *Chill*1 backcross was conducted. In our data, we see WT and the *chill*1 backcross have similar stomatal conductance at 400 ppm and respond in the same magnitude and form to low CO_2 (150ppm) as WT control. Moreover, When the F1-generation *chill*1 backcross is exposed to high CO_2 (900ppm), the stomatal conductance drops as does the WT control. Looking at (Figure 1.3. B & C), *chill*1 and the F1-generation Bd21-3 x *chill*1 backcross respond differently to high CO_2. Thermal imaging data and gas exchange analysis of the F1-generation Bd21-3 x *chill*1 backcross in (Figure 1.3) indicate the causative mutation is recessive.

Similarly, to determine if the causative mutation of *chill*10 is dominant or recessive, gas exchange analysis was conducted on the F1-generation Bd21-3 x *chill* 10 (Figure 1.4). We began by first conducting gas exchange analysis on WT and *chill* 10 (Figure 1.4 A). When both plants were exposed to 400ppm, *chill* 10 seemed to have an increase in stomatal conductance, whereas WT plant showed no change in stomatal conductance. Once plants are exposed to low CO_2 (150ppm), both *chill* 10 and WT showed an increase in stomatal conductance. Interestingly enough, *chill* 10 seemed to show an uninterrupted increase in its stomatal conductance from 400

ppm to 150 ppm. Moreover, when *chill* 10 was exposed to high CO_2, a decrease in stomatal conductance was observed. The stomatal conductance of *chill* 10 after exposure to high CO_2 did decrease as did WT, but the overall stomatal conductance was higher than WT's. By analyzing the normalized data of the average gas exchange of the first 10 minutes in (Figure 1.3.B), the change in stomatal conductance of *chill* 10 after exposure to high CO_2 (900ppm) compared to WT was of less magnitude and arrived at its endpoint much more rapidly. Similarly, gas exchange analysis was conducted on WT and the F1-generation Bd21-3 x *chill* 10 backcross (Figure 1.4.C & D). In (Figure 1.4.C.) when WT and the F1-generation Bd21-3 x *chill* 10 backcross were initially exposed to ambient CO_2 (400ppm), the F1 *chill* 10 backcross had a similar increase in stomatal conductance compared to *chill* 10, but also started with an overall increased stomatal conductance. Then, when both plants were exposed to low CO_2 (150ppm), WT and the F1 *chill* 10 backcross both showed an increase in stomatal conductance. In (Figure 1.4.D) the relative increase in stomatal conductance at 150ppm of the F1 *chill* 10 backcross was similar in magnitude to WT. When the F1-generation Bd21-3 x *chill* 10 backcross was exposed to high CO_2 (900ppm) in (Figure 1.4.D), stomatal conductance did drop as did WT, but similarly to the extent as seen in the *chill* 10 mutant. Gas exchange analysis of *chill 10*, WT, and the F1-generation Bd21-3 x *chill* 10 backcross suggest the causative mutation is semi-dominant.

To determine the causative mutation of chill 15, an F1 generation backcross was generated by crossing *chill*15 with the parental line, Bd21-3. To determine if the causative mutation is dominant or recessive, phenotypic assays were conducted on the F1-generation Bd21-3 x *chill* 15 backcross. Thermal imaging after exposure to high CO_2 was conducted to determine if the F1-generation Bd21-3 x *chill* 15 backcross would have a similar cool leaf temperature as *chill* 15 or a WT-like leaf temperature. Shown in (Figure 1.5.A) is a thermal image of WT, *Chill* 15, and

Bd21-3 x *Chill* 15 after exposure to high CO_2. *Chill* 15 and Bd21-3 x *Chill* 15 showed a cooler leaf temperature relative to WT, while all pots seemed to have similar soil moisture. The *Chill* 15 and Bd21-3 x *Chill* 15 plants showed leaves to be very cold compared to other leaves within the respective plants. Although the WT plant seemed to have some cool leaf tips, it had an overall warmer leaf temperature compared to the mutant plants. To determine if the causative mutation of *chill* 15 is dominant or recessive, further tests had to be conducted. Shown in (Figure 1.5.B) are WT and *chill* 15 stomatal conductance measurements plants in response to [CO_2]-shifts. Both WT and *chill* 15 plants had similar stomatal conductance at 400ppm and responded alike with an increase in stomatal conductance when exposed to low CO_2 (150ppm). When *chill* 15 and WT were exposed to high CO_2 (900ppm), both plants show a decrease in stomatal conductance. However, the response of *chill* 15 was slower than WT and the magnitude of decrease in stomatal conductance was lower. Moreover, when gas exchange analysis was conducted on the F1-generation of Bd21-3 x *chill* 15 (Figure 1.5.C), it showed similar responses to [CO_2]-shifts as *chill* 15. Similarly, to *chill* 15, Bd21-3 x *chill* 15 had the same stomatal conductance as WT at the beginning of the experiment when plants were exposed to 400 ppm. When the plants are exposed to low CO_2 (150ppm), Bd21-3 x *chill* 15 responded like WT, with similar increase in stomatal conductance. However, when both WT and Bd21-3 x *chill* 15 were exposed to high CO_2, the degree to which a decrease in stomatal conductance occurs was different in both plants. Bd21-3 x *chill* 15 did respond to 900 ppm by decreasing stomatal conductance just like *chill* 15 but seemed to have a slower and weaker response to 900ppm than *chill* 15. Looking at thermal imaging after exposure to high CO_2 (900ppm) and gas exchange analysis of WT, Bd21-3 and F1-generation Bd21-3 x *chill* 15 backcross in response to [CO_2]-shifts, the data suggest the causative mutation of *chill* 15 is dominant.

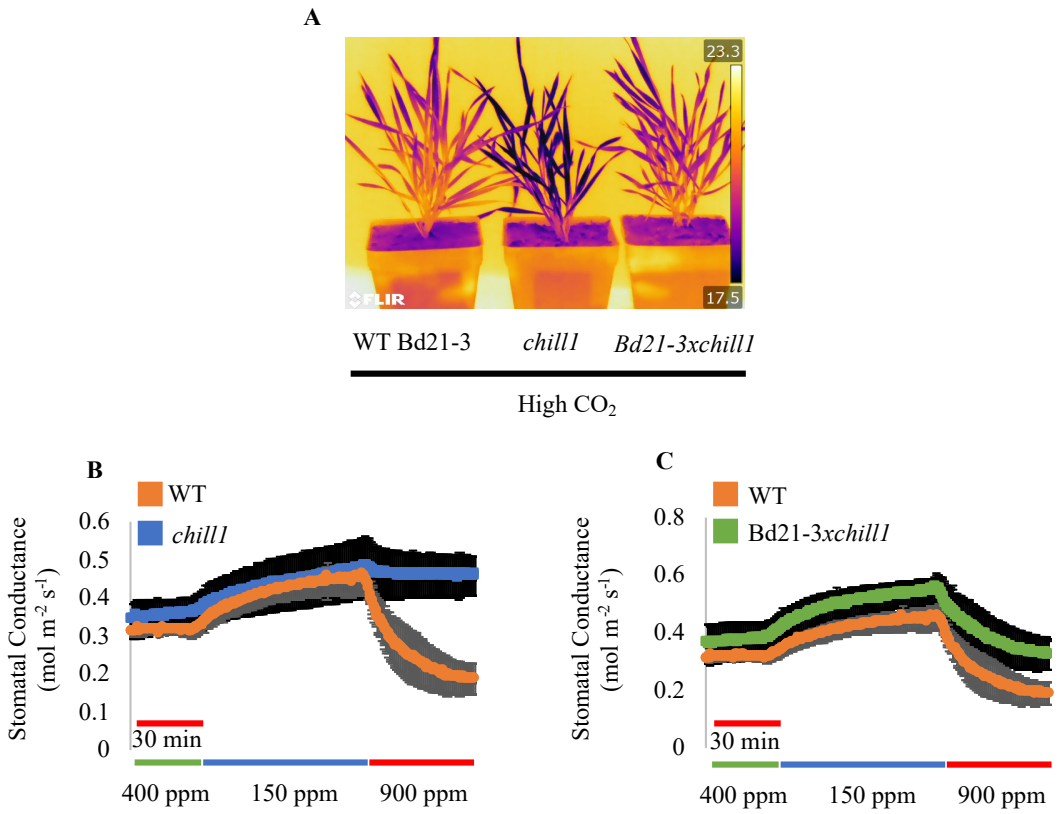

Figure 1.3.: Thermal imaging and Gas Exchange analysis of *chill* 1 and Bd21-3 x *chill* 1 F1-generation backcross suggest *chill* 1 mutant phenotype is recessive. (A) Thermal imaging of parallel grown wild-type control, *chill* 1, and Bd21-3 x *chill* 1 backcross after exposure to high CO_2 (900ppm) for 3 hours. Bd21-3 x *chill* 1 shows a wild-type-like canopy leaf temperature, whereas *chill* 1 shows a cooler leaf temperature. (B) Stomatal conductance (gs) of parallel grown wild-type, *chill* 1 was analyzed using a gas exchange analyzer. Data are the average of n=3 ±SEM experiments, four leaves per experiment (=12 leaves total per genotype). (C) The stomatal conductance (gs) of parallel grown wild-type control, and Bd21-3 x *chill* 1 backcross leaves was analyzed using a gas exchange analyzer. Data are the average of n = 3 ±SEM experiments, four leaves per experiment (=12 leaves total per genotype).

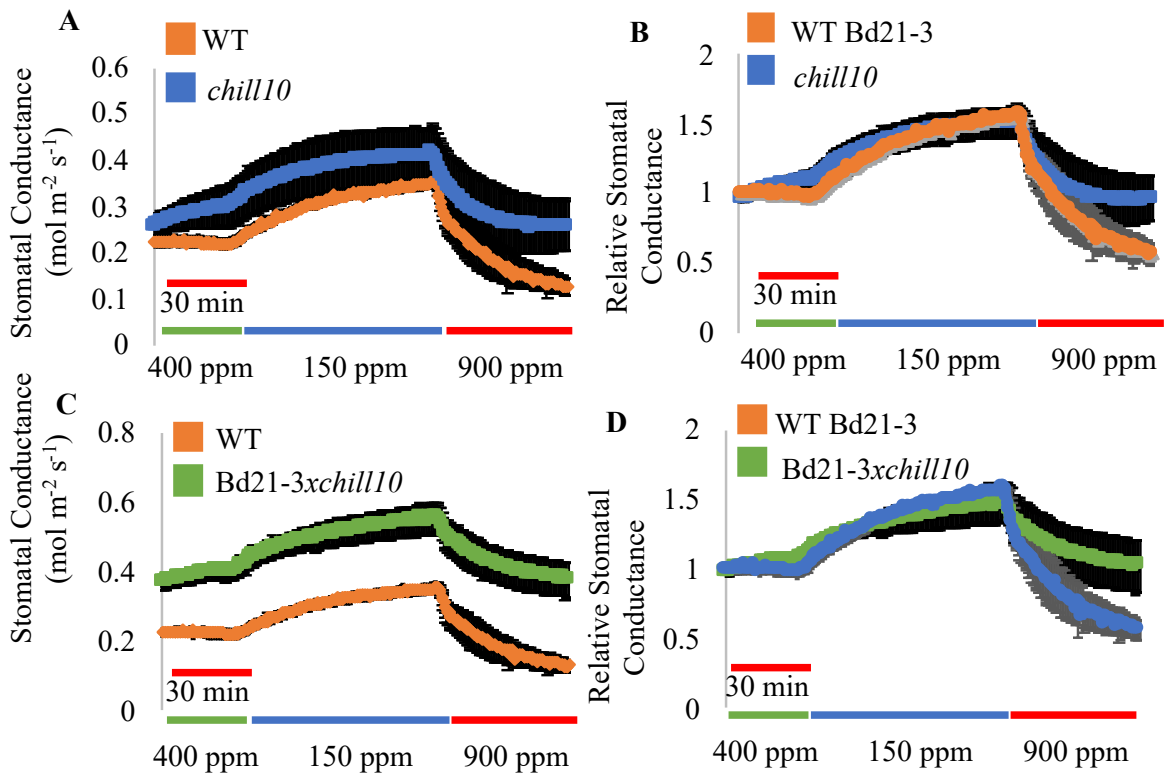

Figure 1.4.: LiCOR gas exchange analysis of *chill* 10 and Bd21-3 x *chill* 10 F1-generation backcross suggest *chill* 10 phenotype is semi-dominant. (A) Stomatal conductance (gs) of parallel grown wild-type control and *chill* 10 was analyzed using a gas exchange analyzer. Data are the average of n=3 ±SEM experiments, four leaves per experiment (=12 leaves total per genotype).). (B) This is the normalized data to the average (gs) of the 10 first minutes of (A). Stomatal conductance (gs) of parallel grown wild-type and Bd21-3 x *chill* 10 backcross was analyzed using a gas exchange analyzer (C). Data are the average of n = 3 ±SEM experiments, four leaves per experiment (=12 leaves total per genotype). (D) This is the normalized data to the average (gs) of the 10 first minutes of (c)

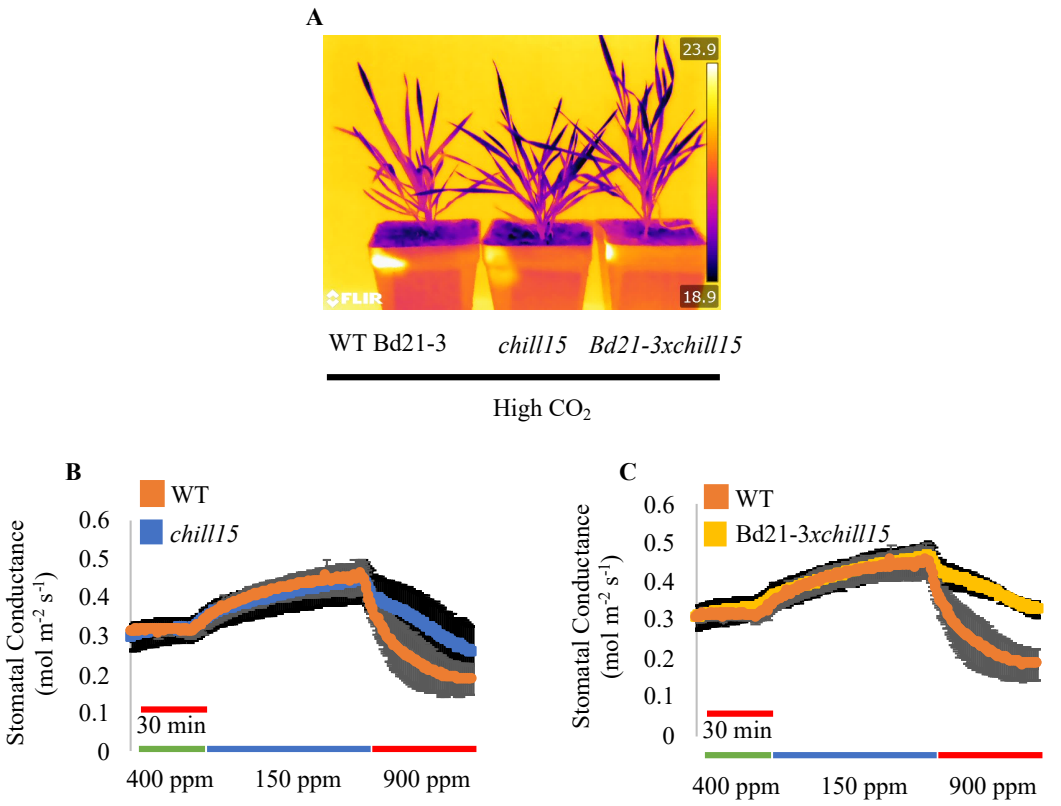

Figure 1.5.: Thermal imaging and Gas Exchange analysis of *chill* 15 and F1-generation Bd21-3 x *chill* 15 suggests the *chill* 15 phenotype is dominant. (A) Thermal imaging of parallel grown plants after exposure to high CO_2 (900ppm) for 3 hours. (B) The stomatal conductance (gs) of parallel grown wild-type and *chill* 15 mutant leaves was analyzed using a gas exchange analyzer. Data are the average of n = 3 ±SEM experiments, four leaves per experiment (=12 leaves total per genotype). (C) The stomatal conductance (gs) of parallel grown Bd21-3 WT and Bd21-3xchill15 backcross Brachypodium leaves was analyzed using a gas exchange analyzer. Data are the average of n = 3 ±SEM experiments, four leaves per experiment (=12 leaves total per genotype)

1.2.4 *Further characterization of chill mutant*

Stomatal pores play a key role in plant transpiration. An increase or decrease in stomatal development can directly affect transpiration rates and, as a result, affect a plants canopy leaf temperature. Furthermore, the size of stomatal pores can affect transpiration by either increasing or reducing stomatal aperture. Therefore, further characterization was conducted on *chill* 9

(Figure 1.6) using gas exchange analysis and DIC stomatal imaging to investigate to what extent does stomatal morphology and development play a role in the phenotype.

In order to investigate how stomatal development or morphology may play a role in the leaf temperature phenotypes of the *chill* mutants, gas exchange analysis and stomatal pore analysis was conducted on *chill* 9. Initially, stomatal conductance was measured in *chill* 9 in response to [CO_2]-shifts (Figure 1.6.A & B). In (Figure 1.6.A), *chill* 9 showed an increase in stomatal conductance when exposed to low CO_2 (150 ppm) and a decrease when exposed to high CO_2 (900 ppm). In addition, *chill* 9 had an overall increased stomatal conductance at 400, 150, and 900 ppm relative to WT. When the stomatal conductance was normalized (Figure 1.6.B), we observed that *chill* 9 response-kinetics to [CO_2]-shifts were the same as WT. In order to determine if *chill* 9 had differences in stomatal development compared to WT, stomatal imaging was conducted using a DIC microscope. Stomatal index ratio was calculated to analyze any differences in the number of stomata per pavement cells found in *chill* 9 compared to WT (Figure 1.6.C). Our results showed that *chill* 9 had similar number of stomatal pores for every pavement cell. Stomatal density per area was calculated to determine the overall number of stomatal pores in a given area for *chill* 9 and WT. Shown in (Figure 1.6.D.) is a bar graph measuring the number of stomata, where *chill* 9 has a reduced number of stomatal pores compared to WT. Next, stomatal imaging was conducted to analyze the stomatal morphology of *chill* 9 mutant. In (Figure 1.6.E) is shown stomatal pore complexes of WT, Bd21-3 and *chill* 9, where both have intact grass stomatal complexes. These include 2 dumbbell shaped guard cells and 2 flanking subsidiary cells. Lastly, to finish analyzing stomatal development and morphology in *chill* 9, stomatal pore length was measured. In (Figure 1.6.F.) a bar graph measuring stomatal pore length is shown of Bd21-3 and *chill* 9. The results showed no

significant difference in stomatal pore length between WT, Bd21-3 and *chill* 9. Further analysis measuring stomatal aperture may lead to understanding how stomatal pores are potentially playing a role in the overall increased stomatal conductance compared to WT, Bd21-3 seen in gas exchange analysis. Future experiments will be conducted to attempt to replicate previous stomatal conductance results.

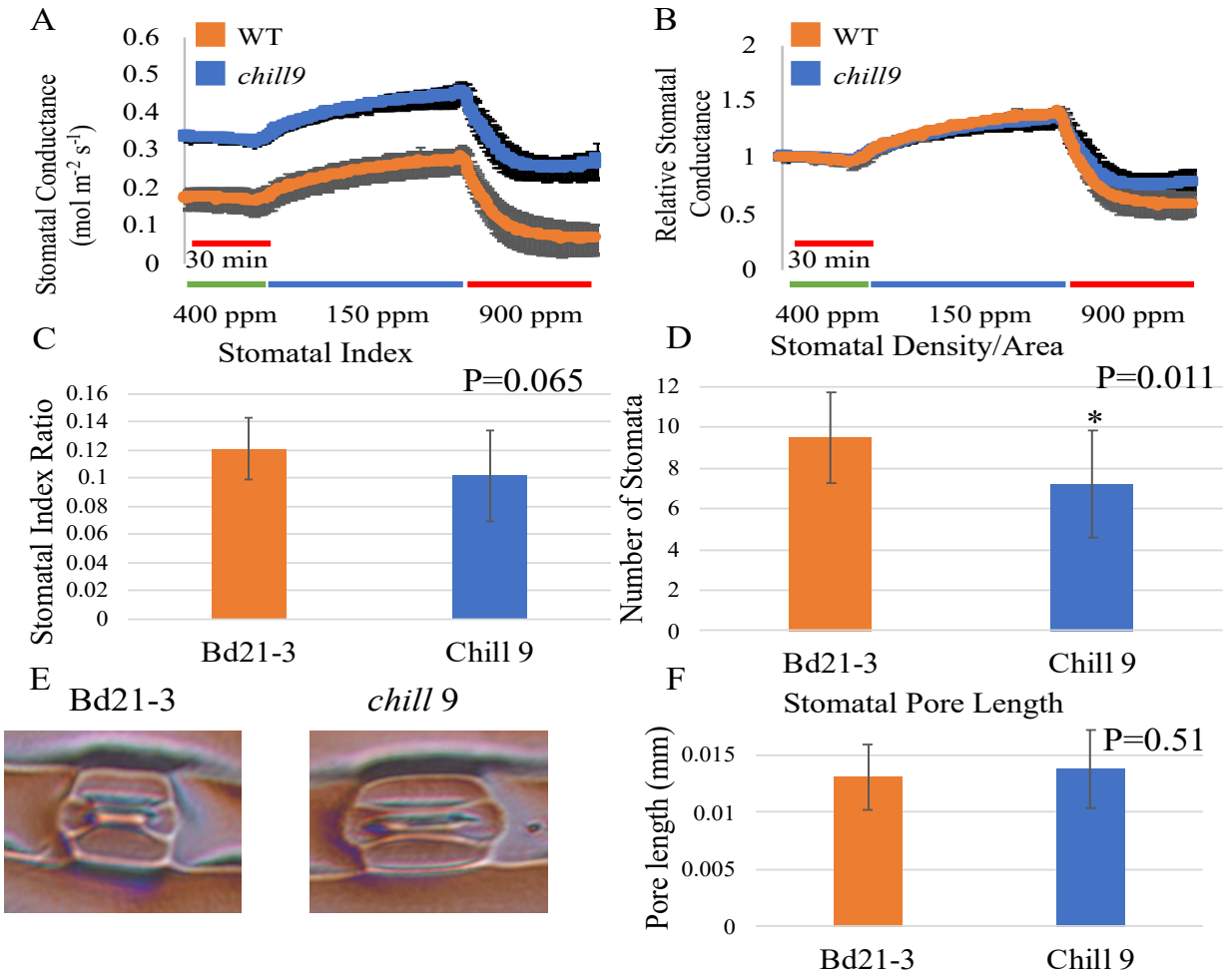

Figure 1.6: Further characterization results of *chill* 9 mutant suggest higher stomatal conductance than Bd21-3, meanwhile wild-type-like stomatal development. (A) Stomatal conductance (gs) of parallel grown wild-type and *chill* 9 was analyzed using a gas exchange analyzer. Data are the average of n = 3 ±SEM experiments, four leaves per experiment (=12 leaves total per genotype). (B) This is the normalized to the average (gs) of the 10 first minutes of (A).
(C) Stomatal index was calculated imaging 4 parallel grown (5-week-old) plants per genotype using DIC imaging. The 4th true leaf from each plant was taken and imaged 4 times at 40x magnification. Each bar represents the average of 4 plants per genotype and error bars represent standard deviation.(D) Using the DIC images from (C), Stomatal density was calculated. (E) DIC images are shown to depict stomatal morphology observed from Bd21-3 and *chill* 9 mutant. (F) Using data from (C), stomatal pore length was calculated by measuring 20 stomata for each genotype. The error bars represent standard deviation.

1.2.5 *Selecting for the F2 mapping population*

One of the two approaches taken to identify the causative mutation of the *chill* mutants was to backcross a respective *chill* mutant with the parental line Bd21-3 and generate an F2 mapping population. In (Figure 1.7 A & C) is shown thermal images of 4-week-old Bd21-3, *chill* 1 and the F2 generation Bd21-3 x *chill* 1 after exposure to high CO_2 (1000ppm) for 4 hours. Bd21-3 and *chill* 1 were thermally images as controls to determine their response to high CO_2. The Bd21-3 control showed a warm canopy leaf temperature, whereas the *chill* 1 plant showed a cool canopy leaf temperature. In (Figure 1.7.A), F2 generation Bd21-3 *chill* 1 plant #1 and #3 show a cool leaf temperature similar to *chill* 1, whereas plant #2 shows a WT-like leaf temperature. In (Figure 1.7.B) colored images of all plants are shown to show they are all healthy plants. Moreover, in (Figure 1.7.C) F2 plant #5 shows a cool leaf temperature similar to *chill* 1. However, F2 plants #4, 6, and 7 show a warm leaf temperature similar to WT. Figure 1.7.D shows the plants in panel C as a photographic image to depict the health of the plants. Plants will be selected and grouped in one of two groups: WT-like leaf temperature phenotype and *Chill* 1-like cool leaf temperature. Both groups will be kept separate and DNA will be extracted for whole genome sequencing.

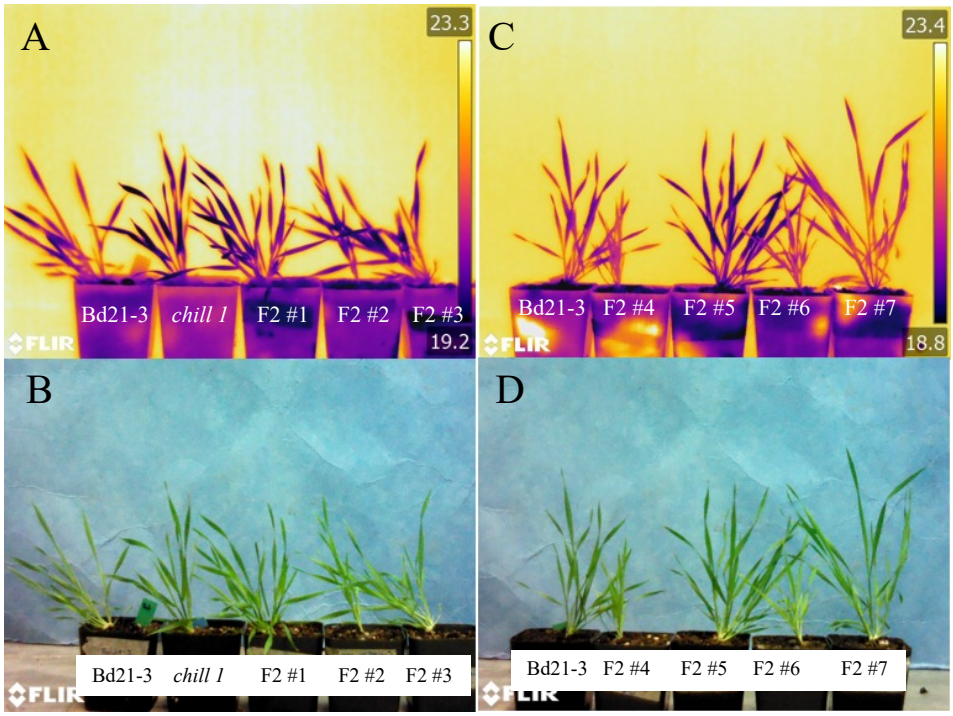

Figure 1.7: Bd21-3 x *chill* 1 F2 mapping Population. Shown are thermal images of 4 week-old, F2-generation Bd21-3 x *chill* 1 backcross imaged next to wild-type control, Bd21-3, and *chill1* after exposure to high CO_2 (1000ppm) for 4 hours. In panel (A & B) WT control, Bd21-3 and *chill* 1 are shown next to F2 population plants 1-3. Plants 1 and 3 show a *chill*1-like leaf temperature, whereas plant 2 shows a WT-like leaf temperature. In panel (C & D) only WT control, Bd21-3, is shown for comparison. Plant 5 shows a *chill*1-like phenotype, whereas plants 4, 6, and 7 show a WT-like leaf temperature. In order to conduct bulk-segregant analysis to identify the causative mutation, the backcrosses will be separated into two groups: wild-type-like canopy leaf temperature and *chill* 1-like canopy leaf temperature. DNA will be extracted, pooled and sent for sequencing.

1.3 Discussion:

Our forward genetic screen used to identify mutants in the grass model, *Brachypodium distachyon*, has shown effectiveness. 21 putative mutants were identified with cooler leaf temperature relative to wild-type controls at ambient CO_2. To date, there has not been a published forward genetic screen for mutants impaired in stomatal movements in grasses. These 21 isolated putative mutants have the potential to identify novel genes and elucidate the CO_2 signaling pathway that regulates stomatal movements in grasses. As a result, this research may facilitate future crop engineering for generating more water-use efficient plants by speeding up or regulating stomatal movements.

Screening over 1000 M5 EMS mutagenized plant lines in our primary screen rendered 50 putative mutants showing a warmer or cooler leaf temperature relative to the WT, Bd21-3 control. After regrowing and retesting these 50 putative mutants in the M5 generation, 28 lines were confirmed. During our initial screen in the M5 generation, our growth conditions were not optimized, meaning plant growth for all plants was not uniform. The average light intensity was below 200 umol $m^{-2}s^{-1}$, the soil mixture used did not promote root growth as well, and it was noticed plants were not watered evenly. Stomatal pores on leaves are important for controlling the intake of CO_2 and loss of water via transpiration. Environmental stimuli like light, water status and temperature affect stomatal conductance. Plants that are not watered well, produce the drought hormone ABA (abscisic acid) (Pei & Kuchitsu, 2005), which leads to stomatal closure to reduce water loss. (Cominelli et al., 2005). Stomatal closure due to the exposure of ABA reduces plant transpiration and, thus, could have played a role in the leaf temperature phenotype we observed in the 22 lines in the primary screen that were not confirmed after regrowing and reimaging in the M5 generation in our secondary screen.

Conducting phenotypic assays on the confirmed 21 *chill* mutants in a tertiary screen in the M6 generation allowed for the mutants to be characterized and grouped based on their leaf temperatures after exposure to high CO_2, their responses to [CO_2]-shifts and stomatal development. Since stomata play a direct role in plant transpiration, stomatal index and density imaging and calculations were conducted to determine whether stomatal development plays a role in the cool leaf phenotype observed in each of the *chill* mutants. Plants with larger sized or more stomatal pores on leaves than other plants have the potential to transpire more and, thus, show a cooler leaf temperature. Our stomatal density and index calculations showed that all mutants had WT-like stomatal development. This suggests that the leaf temperature phenotype found in the M6 generation is not due to stomatal development. Although we determined the average number of stomatal pores per given area (stomatal density) and the number of stomata per pavement cell (stomatal index) to be the same for the *chill* mutants and WT, Bd21-3, further characterization of stomatal pore length, guard cell aperture and subsidiary cell size will need to be conducted. These three different characteristics may give us more insight if a given cell type is playing a role in the leaf temperature we measure in the *chill* mutants.

To further characterize the M6 generation of the *chill* mutants, plants were exposed to high CO_2 (900ppm) and imaged afterwards using a thermal imaging camera. High CO_2 is a stimulus that has a short-term effect on plants by inducing stomatal closure and, thus, raising leaf temperature (Hashimoto et al., 2006; Roelfsema, Hanstein, Felle, & Hedrich, 2002). Exposing plants to high CO_2 allows us to identify plants that are potentially insensitive to CO_2. Our thermal imaging data after exposure to high CO_2 indicates 8 of the 21 confirmed *chill* mutants show a cooler leaf temperature relative to the WT control after high CO_2 treatment. These 8 *chill* mutants (*chill* 1, 2, 3, 4, 5, 10, 15, 16) have great potential of giving us insight on elements

involved in CO_2-dependent stomatal regulation in grasses. Thermal imaging is a great tool for objective analysis of plant transpiration via canopy leaf temperature. However, plant transpiration via stomatal pores is one of various factors that can affect the overall leaf temperature observed using an infrared thermal imaging camera. For example, mutants with reduced waxy cuticles can also have differences in transpiration and, thus, show a difference in leaf temperature using a thermal camera. The reason is that a waxy cuticle functions to obstruct uncontrolled water loss (Kosma & Jenks, 2007). The highly expressed HIGH CARBON DIOXIDE (*hic*) gene in guard cells, encodes an enzyme that plays a key role in the production of waxy cuticles (Casson & Hetherington, 2010). Therefore, further characterization of all mutants needs to be done, to determine if there are differences in leaf waxiness relative to the WT parent line, Bd21-3.

To further characterize the *chill* mutants, gas exchange analysis was conducted to gain insight on how the *chill* mutants respond to [CO_2] shifts by measuring stomatal conductance. Further characterization of the 21 *chill* mutants using Gas exchange analysis enabled us to group the mutants based on their response-type to [CO_2] shifts. Group 1 consists of *chill* 1, 10, 15 and potentially 11, and 12 showing impairments to [CO_2] shifts. CO_2 and ABA signaling pathway have been shown in our laboratory to have crosstalk to coordinate stomatal movements. The *SLAC*1 gene encodes an anion channel expressed in guard cells that is responsible for the release of solutes, resulting in the decrease of guard cell turgidity and stomatal closure. The *SLAC*1 mutant does not respond to CO_2 and ABA, which results in constant cooler leaf temperature. To determine if the causative mutation related to the CO_2-shift insensitivity phenotype in *chill* 1 and 15 is CO_2 specific, stomatal responses to small soluble molecule ABA was conducted. *Chill* 1 and 15 showed a WT-like response (data not shown), suggesting the observed phenotype is CO_2

specific. Group 2 refers to mutants with distinct kinetics of stomatal responses to [CO_2] shifts: candidates 11, 12 and potentially 21. These mutants have similar stomatal conductance as the WT control. With this in mind, understanding the causative mutation of these *chill* mutants and the function of the encoded protein may lead to understanding the proteins involved in transducing the signal for stomatal movements. Group 3 (*chill* 3, 11, 12) and 4 (*chill* 6, 9, 14, 17, 19) refer to mutants that show a lower or higher, respectfully, steady-state stomatal conductance relative to WT, Bd21-3. Our stomatal index and density data show all mutants with similar stomatal development as wild type, suggesting that differences in stomatal patterning or stomatal pore size are potentially at play. Lastly, group 5 (*chill* 2, 9, 13) refers to mutants showing potential stomatal re-opening at high CO_2. In our lab it has been shown that CO_2 can induce stomatal closure, but ABA is necessary to maintain closed stomata or inhibit stomatal opening. Further experiments will be conducted to determine the endogenous concentration of ABA in these mutants.

Thermography is a tool that has been successful at identifying mutants with impaired stomatal responses to stimuli, such as light, CO_2, and ABA (Hashimoto et al., 2006; Merlot et al., 2002; Negi et al., 2014). *Abi1* and *ost*1 mutants have been shown to have a cooler leaf temperature under drought conditions relative to the WT, due to their inability to close their stomata after being exposed to drought (Merlot et al., 2002). After the 21 *chill* mutants were confirmed in the M6 generation and characterized, research towards identifying the causative mutation was undertaken. Two approaches have been taken to map the causative mutation of the *chill* mutants: whole genome sequencing paired with bioinformatics tools and backcrossing *chill* mutants with the parental line to generate an F2 mapping population for bulk-segregant analysis. *Chill* 1, 10, and 15 were backcrossed with the parental line, Bd21-3. Initial phenotypic tests were

conducted on the F1-generation backcrosses to determine if the mutation is recessive or dominant. After exposing the F1-generation Bd21-3 x *chill* 1 backcross to high CO_2, it shows a WT-like leaf temperature. This suggests that the causative mutation of *chill* 1 is recessive, but to further test this, gas exchange analysis was conducted. The F1-generation Bd21-3 x *chill* 1 backcross has similar steady-state stomatal conductance as WT, Bd21-3 at 400ppm. When it is exposed to low CO_2 (150ppm) it increases stomatal conductance like WT. Similarly, after exposure to high CO_2 (900ppm) the *chill* 1 backcross reduces its stomatal conductance. All together with thermal imaging after high CO2, and gas exchange analysis of the F1-generation Bd21-3 x *chill* 1 backcross, we see that the causative mutation of *chill* 1 is recessive. This suggests, according to mendelian genetics, when selecting for the F2 mapping population, we expect ¼ of the plants to show a cool leaf temperature, whereas ¾ of the plants will show a WT-like, warm, leaf temperature after exposure to high CO_2.

To continue with determining if the causative mutation of the rest of the F1-generation backcrosses is dominant or recessive, phenotypic assays were conducted on Bd21-3 x *chill* 15. Similarly, thermal imaging was conducted after exposure to high CO_2 (900ppm) and gas exchange analysis to examine stomatal conductance in response to [CO_2]-shifts. F1-generation Bd21-3 x *chill* 15 shows a cooler leaf temperature relative to the WT control after exposure to high CO_2 similar to *chill* 15. Moreover, gas exchange analysis of F1-generation Bd21-3 x *chill* 15 backcross shows responses similar to *chill* 15. At 400ppm, both Bd21-3 x *chill* 15 and WT, Bd21-3 have similar steady-state stomatal conductance and increase their conductance after exposure to low CO_2 (150ppm). However, when exposed to high CO_2, Bd21-3 x *chill* 15 shows a slow and low magnitude decrease in stomatal conductance relative to WT. These phenotypic assays on the F1-generation of Bd21-3 x *chill* 15 suggests that the causative mutation is

dominant. In order to use the F2 mapping population to generate two bulks: WT-like and *chill* 15 like, we expect to see 3 out of every 4 of the plants to show a cooler leaf temperature relative to WT. The issue that arises when conducting bulk segregant analysis to identify a dominant mutation is that only 1 out of every 3 of the plants showing a cooler leaf temperature relative to WT after exposure to high CO_2 will be homozygous. Only these plants can be used to extract DNA and sent for whole genome sequencing. Further experiments will be conducted to determine the best approach of differentiating the 1/3 of the cool leaf plants, that can be used for Bulk segregant analysis, from the other 2/3 of the plants that also show a cool leaf temperature after exposure to high CO_2. Using bulk-segregant analysis mapping has been used in the past to identify several genes and quantitative trait locus, (QTLs) (Xia et al., 2012) in the grass model, *Brachypodium distachyon.* For example, bulk segregant analysis was used previously to identify a gene (*VRN1*) that plays a role in vernalization (Woods et al., 2017).

The *chill* mutants identified in the EMS-mutagenized *Brachypodium distachyon* plant lines have shown robust phenotypes and carry the ability to provide insight in the CO_2 signaling pathway that can help crop engineers improve crop plants. Lastly, to determine if our screen is effective at identifying putative mutants that play a role in CO_2-dependent stomatal movements, a proof-of-concept investigation will be pursued by ordering sequence-indexed sodium-azide lines for known genes that play a role in stomatal movements.

1.4 Methods:

1. Plant Material & Growth conditions
2. Infra-red Thermal Imaging Analysis
3. DIC imaging and stomatal analysis
4. Licor Gas Exchange

1.4.1 *Plant Material & Growth conditions*:

An M5 generation Ethyl methanesulfonate (EMS) mutagenized seed library of 1075 *Brachypodium distachyon* plant lines of the Bd21-3 ecotype were sent from the Joint Genome Institute (JGI). Bd21-3 was used as WT control for all experiments described in chapter 1. Before potting, seeds were initially placed on plates and cold-treated for 7 days minimum at 4°C . The soil mixture consisted of a 1:1 ratio of vermiculite to perlite. This mixture of vermiculite and perlite was added in order to increase the water retention of the soil. Individual germinated seeds for each genotype were potted in individual small pots. Light intensity in the growth room was set to 250 μE m^{-2} s^{-1} to improve the growth conditions. Plants were exposed to an average atmospheric CO_2 of 450ppm and a 16-hour light/8-hour dark cycle. To maintain a consistent level of soil moisture, plants are given a minimum of 1L of water with added fertilizer every other day.

1.4.2 *Infra-red Thermal Imaging Analysis*:

Thermal imaging was conducted on plants that were 5-6 weeks old using a FLIR Thermal Imaging camera T650sc (FLIR Systems, Inc. Wilsonville, OR 97070 USA). Ambient CO_2 thermal imaging took place in the growth room where the plants were grown. High CO_2 thermal imaging was conducted after plants were exposed to 900 ppm in a Percival, E-36HO, high cO_2

chamber for 3 hours. Both WT and EMS mutagenized plant lines were grown in parallel and under the same conditions. Plants grown for our forward genetic screen were grown in batches to screen more lines as efficiently as possible.

1.4.3 *DIC Imaging and Stomatal analysis*

Stomatal imaging was conducted using an epidermal peel technique developed by Morgana Sidhom and myself. 5-6-week-old plants were used to determine stomatal density and index. First, we remove the 4th true leaf and apply a small dot of glue (Loctite Super Glue) on a slide. We set the center of the leaf on the dot of glue and press down as evenly as possible to prevent formation of an air bubble. Once the glue has hardened, we gently peel off the leaf from the slide and image the impression on the slide using a Differential Interference Contrast (DIC) microscope with a camera. The image is taken at 40x magnification and four images are taken per slide. Stomatal pores and pavement cells were counted if fully contained within the image using the "cell-counter" tool from ImageJ.

1.4.4 *Licor Gas Exchange:*

Stomatal conductance (gs) was measured in leaves of healthy 5- to 6-week-old plants using portable gas exchange system (LI-6800, LI-COR, Lincoln, NE, USA). To prepare plant gas exchange analyses, 4 healthy leaves from each plant were taped together using micropore tape (3M), without damaging, with the abaxial side facing downwards (Ceciliato et al., 2019). Leaves were then equilibrated for 1 hour at [CO_2] of 400 ppm, light intensity of 250 μmol m^{-2} s^{-1} and 65

% humidity. Before beginning to record measurements, we standardized the stomatal conductance to obtain a steady state reading at 400ppm. The data presented represent the average of n= 3 ±SEM experiments, four leaves per experiment (=12 leaves total per genotype).

Chapter 2: Can we increase stomatal development in grass model by downregulating SBT 1.7 genes?

2.1 Introduction:

Stomata play a key role in controlling water loss of plants, the immune response by reducing pathogen entry. For plants, stomatal patterning is an important trait. Generating plants with stomatal pores on the top (adaxial) and bottom (abaxial) of the epidermal leaf, can lead to an increase in water loss and can make plants more vulnerable to pathogens, but can also lead to an increase in CO_2 intake and photosynthetic efficiency (Muir et al., 2015). Therefore, understanding the right ratio of adaxial/abaxial patterning to have on plants may differ for plants based on their environmental growth conditions. If we want plants with an increase in CO_2 intake, we can increase the size or number of stomatal pores, whereas if we want plants to survive better during droughts, we may look at reducing stomatal development.

Our knowledge of stomatal development is currently mainly limited to the model dicot, *Arabidopsis thaliana.* Scientists have been very successful at characterizing different signaling components of stomatal development, movements, pathogen defense and resistance to various abiotic stresses in Arabidopsis. However, *Arabidopsis thaliana* has certain limitations that cannot be addressed in a monocot plant. One of the limitations dicots have relative to monocots, is the way their stomatal complexes are formed. As grasses have unique dumbbell shaped stomata with subsidiary cells, grasses such as *Brachypodium distachyon* can work better as a plant model for investigating stomatal development in crops such as maize, barley and wheat compared to *Arabidopsis thaliana.* Cultivated monocot grasses like wheat and rice provide the majority of human nutrition (Hepworth et al., 2018). Therefore, research on grass stomata could be of critical importance for improving food security

There is a great need for a grass model. Model systems are advantageous because they provide scientists with the ability to investigate processes that are difficult to study in nonmodel organisms (Brkljacic et al., 2011). *Brachypodium distachyon* is a monocot and possesses one of

the smallest grass genomes, at 272Mb (Brkljacic et al., 2011). Rice (*Oryza sativa*) and maize (*Zea mays*) have advantages as grass models, including sequenced genomes, and a plethora of resources (http://www.gramene.org/ and http://www.maizegdb.org/). The major challenges associated with these species pertains to the large size of the plants, generation time, in maize the large genome and the specialized conditions required to grow healthy plants (Jung et al., 2008). *Brachypodium distachyon* is similar to rice, wheat, and Barley in that, it uses the C_3 photosynthetic pathway (Brkljacic et al., 2011). Some advantages of Brachypodium is that it is very easy to work with, it is small in stature, short generation time, small genome, it can self-pollinate, and is easily grown under optimized growth room conditions. (Draper et al., 2001).

The elements involved in stomatal development in *Arabidopsis thaliana* have been shown to be transcription factors known as basic helix-loop-helix (bHLH), signaling peptides, receptors and a mitogen-activated protein kinase (MAPK) cascade (Lau & Bergmann, 2012). Stomata originate from specialized cell lineages that are found in young leaves (Bergmann & Sack, 2007). The specialized cell begins its formation with an asymmetric division and becomes a precursor $cell_2$ called the meristemoid. The following step is a symmetric division that generates two cells that will form the stomatal pore (Bergmann & Sack, 2007). Sequence and functional analysis indicates many plants, have conserved transcription factors that play a role in stomatal development (Macalister & Bergmann, 2011). Some of the conserved transcription factors that play a role in stomatal development are AtSPEECHLESS (AtSPCH), AtMUTE, and AtFAMA, which specifically initiate continous asymmetric entry divisions of precursor cells, commitment to stomatal fate and differentiation of guard cells, respectively (McKown & Bergmann, 2020). In order for these transcription factors to function, they require heterodimerisation with IIIb bHLH members, AtICE1 and AtSCREAM2 (AtSCRM2) (Kanaoka

et al., 2008). In plants, stomatal development follows a "one-cell spacing rule" (Geisler et al., 2000), which allows for optimized gas exchange.

It has been shown that signaling peptides play a role in positively and negatively regulating stomatal development. A family of cysteine-rich intracellular peptides signals, known as EPIDERMAL PATTERNING FACTORS (EPFs and EPF-like (EPFLs)) regulate stomatal development in *Arabidopsis thaliana* (Richardson & Torii, 2013). Specifically, EPF1 and EPF2 negatively regulate stomatal development by activation receptor kinases, whereas STOMAGEN(EPFL9) positively regulates stomatal development by competing for binding to receptor kinases with EPF1/2 (Zoulias et al., 2018). Once the EPF 1/2 peptide binds to the receptor kinase, the signal is transduced via the ERF/TMM/SERK receptor complex, activating a MAP Kinase cascade that, ultimately, results in the negative regulation of the transcription factor SPCH (Zoulias et al., 2018). More specifically, a protein kinase known as (MAPKKK) YODA (AtYDA) (Bergmann et al., 2004), relays this information through downstream kinases (Lampard et al., 2009) resulting in the inhibition of SPEECHLESS (AtSPCH) via phosphorylation (Lampard et al., 2008).

Environmental factors such as CO_2 have been shown to affect stomatal development. For example, in Arabidopsis, the subtilisin protease, CO_2 RESPONSE SECRETED PROTEASE (CRSP), plays a role in CO_2-dependent regulation of stomatal development in response to higher CO_2 levels and can cleave the EPF2 propeptide (Engineer et al., 2014), resulting in downregulation of stomatal development.

Plants defective in the HIGH CARBON DIOXIDE (HIC) mutant showed an increase in the number of stomatal pores, when grown at high CO_2, rather than a decrease (Casson & Hetherington, 2010). The *HIC* gene is expressed in guard cells and encodes an enzyme that

functions to produce fatty acid components necessary for plant extracellular matrix and waxy cuticle formation. Despite this advance, it remains unclear how *hic* functions to regulate stomatal development. Additionally, another long-known subtilisin protease, STOMATAL DENSITY DEFICIENT (SDD1), has an impact on stomatal density in Arabidopsis and maize (Von Groll et al., 2002). The Arabidopsis mutant stomatal density and distribution1-1 (sdd1-1), displays stomata clustering and up to a fourfold increase in the number of stomata (Von Groll et al., 2002).

Subtilisin-like proteases have been shown to play a role in CO_2-dependent stomatal development regulation by activating peptide signals that regulate stomatal development in *Arabidopsis thaliana*. However, whether and which gene family members of these proteases affect stomatal density and development in grasses remains unknown. In this reverse genetic approach, we investigated whether downregulating Subtilisin-like proteases (SBT 1.7), identified by proteomic and transcriptomic analyses in developing leaves, using artificial microRNAs, affect stomatal development in a grass model, *Brachypodium distachyon*.

2.2 Results:

2.2.1 *Identifying SBT genes to Downregulate*

Understanding the different signals and elements involved in stomatal development can be of interest to be able to generate plants with increased stomatal density for a resulting increase in CO_2 intake or a decrease in stomatal density to reduce water loss via transpiration. In *Arabidopsis thaliana*, Subitlisin-like serine proteases (SBT's) have been shown to cleave and activate peptide signals, that play a role in regulating stomatal development (Berger & Altmann, 2000) Engineer et al., 2014). To identify which SBT genes may play a role in stomatal development in *Brachypodium* distachyon, apoplast proteomic analysis was conducted. Results indicated that SBT 1.7 genes are highly expressed in leaves throughout plant development. As a result, it was decided to downregulate two genes from the SBT 1.7 gene family using a plasmid containing an artificial microRNA targeting (Bradi1g07840 & Bradi1g14860) (Figure 2.3). The plasmids were designed by Dr. Felix Hauser and cloned by Dr. Sebastian Schulze. Both plasmids target the same two SBT 1.7 genes but differ in the promoters driving the expression of the plasmid. pSES322-plasmid contains a maize ubiquitin promoter whereas, pSES331-plasmid contains two 35s promoters. To generate the T0 population, Bd21-3 ecotype was transformed with either plasmid by Boyce Thompson Institute Biotechnology Center via agrobacterium transformation.

MicroRNAs (miRNAs) are small RNAs that are roughly 21 nucleotides long that play a role in regulating expression of genes (Bartel, 2004). Artificial microRNA's can be designed and function just like naturally occurring miRNAs to silence specific gene(s). The way microRNAs silence the expression of a gene is to an enzyme known as Dicer cleaves double-stranded RNA. The cleaved RNA is then loaded into a protein called argonaute, which target complementary

sequences (Bologna & Voinnet, 2014). Conducting a reverse genetic screen using artificial microRNAs to silence genes has the potential to have homologues off-targets. Our artificial microRNA is a 21-nucleotide sequence: 5' GAAGAACTCCACGGGCGTCCA 3'. To determine what potential homologs of the target genes may be targeted by the artificial microRNA, a phylogenetic tree was generated (Figure 2.1). 17 potential off-target homolog proteins of the SBT 1.7-targeting artificial microRNA were identified using JGI's Jbrowse tool. The closest homolog is the 3rd gene in the SBT 1.7 gene family (Bradi1g14860, Bradi1g07840 & Bradi4g24790), making it a great control for examining specificity of the artificial microRNA used to downregulate the target genes. To first determine if we could use the 3rd gene in the SBT 1.7 gene family (Bradi4g24790), the expression levels of the transcript at low (150ppm) and high CO_2 (900ppm) was checked (Figure 2.2). Our results showed that the 3rd SBT gene in the SBT 1.7 family (Bradi4g24790) is expressed at very low levels at low and high CO_2 (Figure 2.2), making it challenging to analyze if and to what extent the artificial microRNA is downregulating it. Therefore, we looked for a close homolog of the target genes that was highly expressed at both high and low CO_2 and found (Bradi2g48740) to be the best next gene to use as control for analyzing the artificial microRNAs specificity.

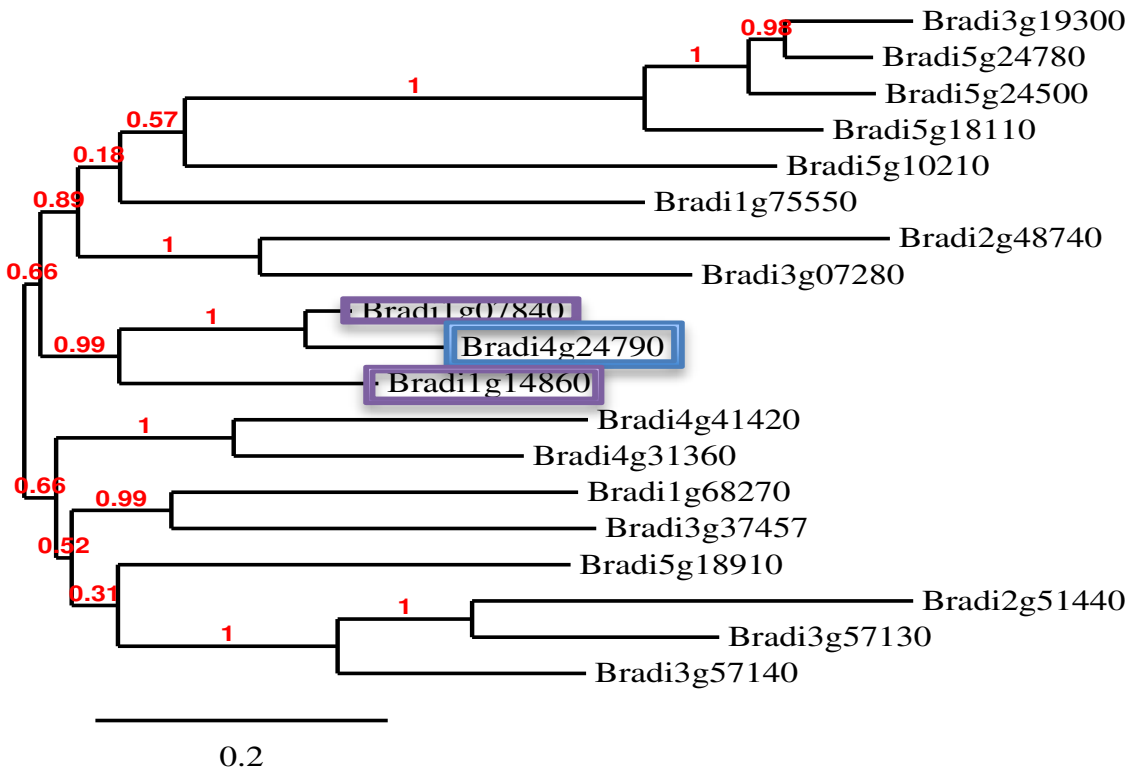

Figure 2.1: Phylogenetic tree of SBT 1.7 homologs in *Brachypodium distachyon*. Shown above is a phylogenetic tree of homologous genes in *Brachypodium distachyon*. To determine potential off-target homolog proteins of the artificial microRNA, JGI's Jbrowse tool was used to determine homologous proteins in Bd21-3 for each of the two target genes, (Bradi1g07840 and Bradi1g14860). The transcript sequences from each homologous protein was taken and entered into a phylogenetic tree generator. Note, although the closest related gene to both the target genes (Bradi1g07840 and Bradi1g14860) was the 3rd gene in the SBT 1.7 family (Bradi4g24790), we could not use it as a control for qPCR tests, due to low transcript expression at low and high CO_2.

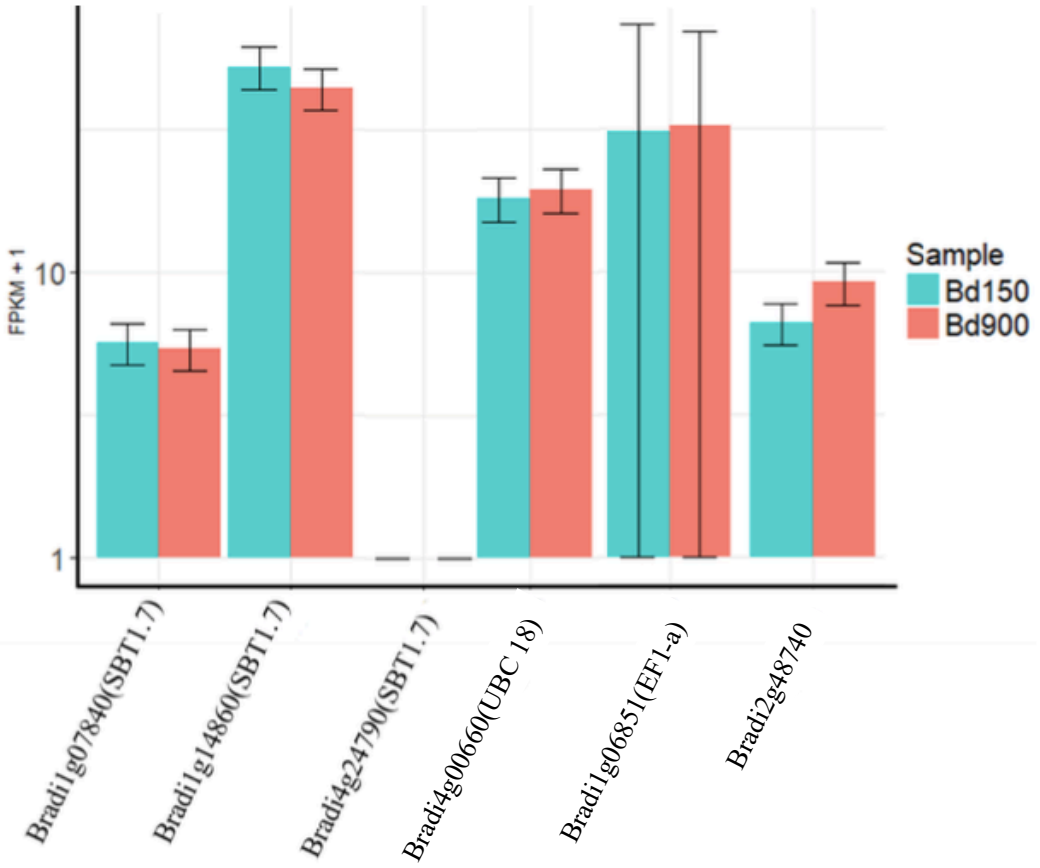

Figure 2.2: Expression levels of selected SBT 1.7 homologues genes, UBC18 & EF1-a housekeeping genes and SBT homolog in *Brachypodium distachyon*. Wild type Bd21-3 plants were exposed to 150 ppm [CO_2] (Bd150) or 900ppm [CO_2] (Bd900). Expression levels of SBT1.7 genes Bradi1g07840, Bradi1g14860, Bradi4g24790 and Bradi2g48740 are shown, as well as expression of the house keeping genes Bradi4g00660 (UBC18) and Bradi1g06851 (EF1α). Our transcriptomic data for Bradi4g24790 showed low expression levels in both high and low CO_2 making it challenging to identify any potential changes due to the artificial microRNA. As a result, we chose an alternative SBT gene, Bradi2g48740.

2.2.2 *Analyzing leaf temperature phenotypes of genotyped transformed plants*

Stomatal pores directly play a role in plant transpiration. Having an increase in stomatal density can lead to an increase in plant transpiration and an increase in leaf cooling. Thermal

imaging was conducted on T2 generation plants transformed with plasmids (Figure 2.3) to investigate if plasmid-containing plants showed a difference in leaf temperature relative to the azygous control. In (Figure 2.4.A) 3 different thermal images of 6-week-old 322 plasmid-containing plants (right plant) were imaged next to the azygous control (left plant) at ambient CO_2. The 322 plasmid-containing plant on the outer left and right (Figure 2.4.A.) seemed to have a cool leaf temperature, whereas the 322 plasmid-containing plant in the middle had a warmer leaf temperature relative to the azygous control. Similarly, in (Figure 2.4.B) the 5-week-old 331 plasmid-containing plant in the middle seemed to have a cooler leaf temperature relative to the azygous control. However, the outer 331 plasmid-containing plants on the left and right showed similar leaf temperature as the azygous control.

Once all plants were thermally imaged, plants were genotyped to determine which plants contained the artificial microRNA. Two approaches were used throughout the entire screen: PCR-based genotyping and screening for hygromycin resistance. The first approach taken to identify plants containing the plasmid was to screen for hygromycin resistance. Both plasmids (Figure 2.3) contain a gene that confers resistance to the antibiotic hygromycin. Therefore, plants containing the plasmid should have resistance to hygromycin. In (Figure 2.5.A.) is shown a 12x12 hygromycin-containing agar plate with tips of leaves from plants transformed with the 322-plasmid. Leaves boxed in red (negative control) represent leaves from plants that were previously genotyped using PCR-based methods and did not show amplification for the artificial microRNA, whereas the leaves boxed in blue (positive control) represent plants that showed amplification for the artificial microRNA. The positive control leaves showed a green leaf color, whereas the negative control leaves showed darkening or brown leaves. Moreover, there are leaves numbered 200-208 that were placed to test for hygromycin resistance. All plants tested for

hygromycin remained green, except 201, 205, 208 and the negative control. To see a better look at the difference between leaves from Bd21-3, a positive and a negative control (Figure 2.5.B), all 3 leaves were imaged 5 days after exposure to hygromycin. Bd21-3 acts as an absolute negative control since it was not transformed with the plasmid containing the hygromycin resistance gene. Both Bd21-3 and the negative control showed a darkening of the leave, meanwhile the positive control remained green.

To conduct a proof-of-concept, we took the same plants from above (Figure 2.5) and extracted DNA to determine which plants showed amplification of the artificial microRNA. In (Figure 2.6) a gel is shown with 9 DNA samples for testing, a WT and positive control. Plants that remained green in the hygromycin resistance screen, 200, 202, 203, 204, 206, 207 and positive control also showed amplification for the artificial microRNA. Similarly, leaves that showed a discoloring in their leaves also showed no amplification for the artificial microRNA like WT, 201, 205 and 208. Further genotyping using PCR-based methods was conducted on plants transformed with the 331-plasmid (Figure 2.7). In the gel image, we see 9 DNA samples, a positive and negative control. All plants 1-9 showed amplification of the 200bp artificial microRNA. Water was used as a negative control to determine if any DNA contamination in the master mix exist.

Figure 2.3: Investigating pSES322 and pSES331 amiRNA lines for co-silencing SBT 1.7 genes in *brachypodium distachyon* stomatal development. Based on our proteomic data sets in Brachypodium, wheat and rice, we decided to co-silence two homologous Brachypodium SBT 1.7, Bradi1g07840 and Bradi1g14860. We received four plants from Boyce Thompson Institute Biotechnology Center transformed with the pSES331 (lines pSES331-1 to 4) and five with the pSES322 (lines pSES322-1 to 5) plasmid constructs targeting Bradi1g07840 and Bradi1g14860 genes from the SBT 1.7 gene family. Seven of nine of these plants set seeds. Each of these plants is predicted to represent independent insertion events. T1 plants were propagated and T2 seeds from each independent insertion line were harvested and kept separated (T2 generation).

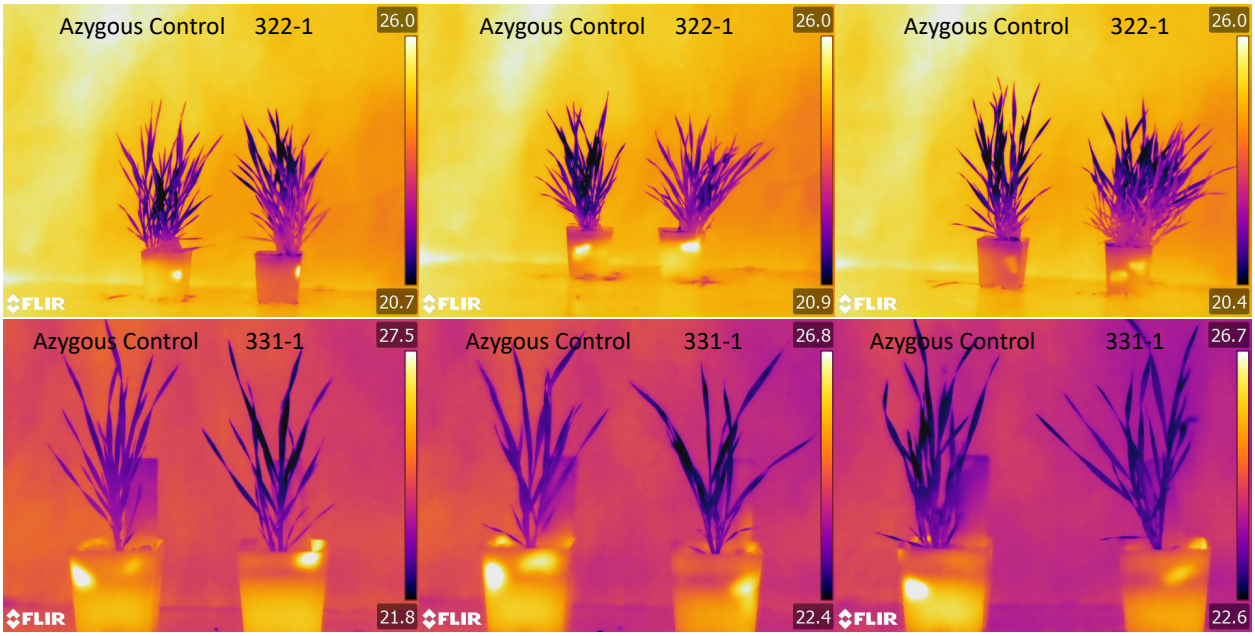

Figure 2.4: Thermal imaging of T2 generation plasmid-containing plants(right) at ambient CO_2 show no robust leaf temperature relative to azygous control. Shown are images using a thermal camera taken of (A) 6-week-old and (B) 5-week-old azygous control plants and plasmid containing plants at ambient CO_2. azygous controls and plasmid containing plants are the same age, respectively, and were grown under the same conditions. The plants were grown under 16/8 light-dark cycle and the light intensity the plants were exposed to was, on average, 300 umol $m^{-2}s^{-1}$.

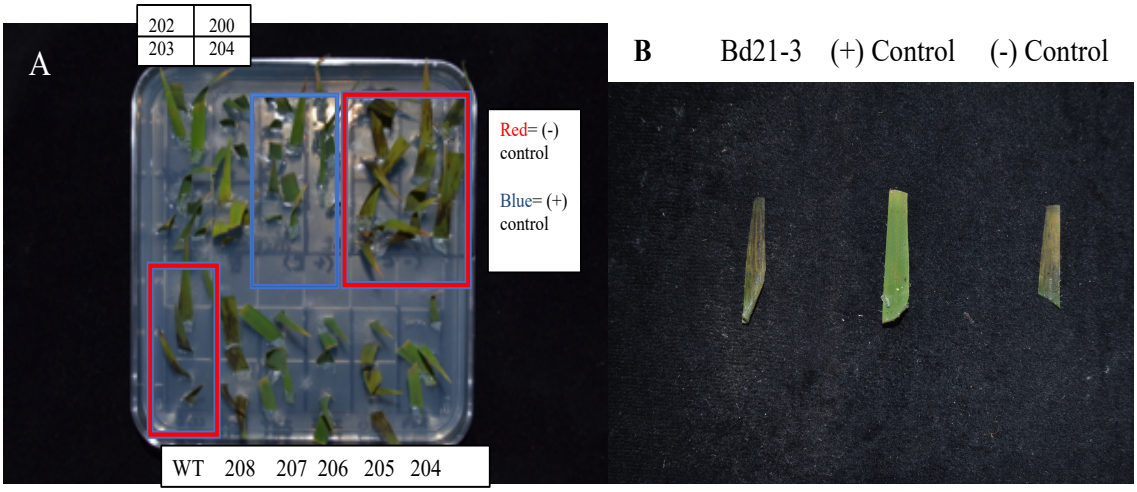

Figure 2.5: Hygromycin Resistance Screen of artificial microRNA transformed assists with identifying plasmid-containing plants. Shown is an experiment investigating hygromycin resistance used to identify plasmid containing plants on the left (A). Panel (B) shows a closer look at the color of leaf tissue from wild-type, Bd21-3, and positive and negative control after 5 days of exposure to hygromycin. Both positive and negative control plants were genotyped via PCR-based genotyping before experiment was conducted to ensure proper controls were being used. 4-5 Healthy leaves from 5-week-old plants were cut and placed on hygromycin-containing agar plates. Images from panel (A & B) were taken 5 days after exposure to hygromycin in agar plates. All leaves showing a darkened color represent transgenic plants that do not contain the amiRNA construct whereas the leaves that maintained a green color do.

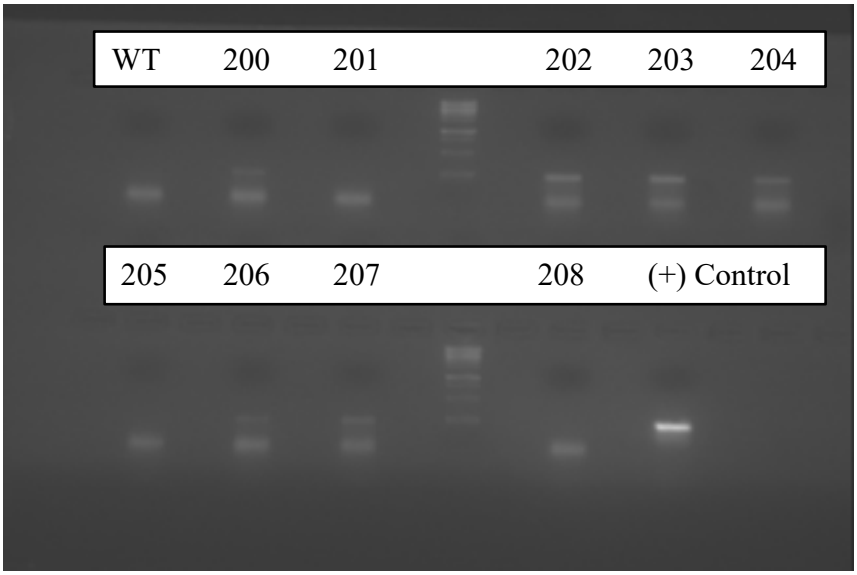

Figure 2.6: PCR-based genotyping of artificial microRNA transformed plants. Shown is an agarose gel showing amplification of the artificial microRNA for independent transformed plants with the 322 plasmid. Leaves from 5-week-old T1 generation plants were taken for DNA extraction using Thermo Fisher's Plant DNAzol reagent. Primers attB2R and att1BF were used to amplify the 200bp artificial microRNA. All plants transformed with the 322-plasmid showed amplification for the artificial microRNA, except plants 201 and 205, 208. Positive control, (+) control, represents purified DNA of the pSES322 plasmid. Note, the lowest band seen in the agarose gel for each well is due to primer dimer.

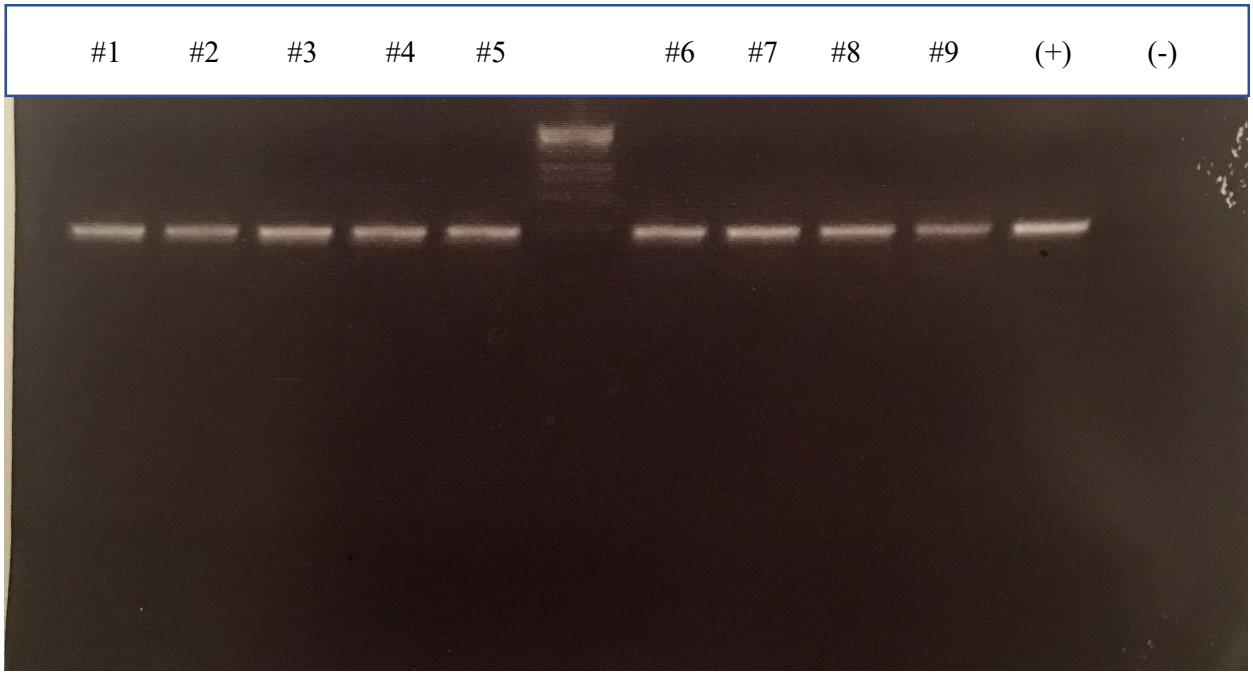

Figure 2.7: PCR-based genotyping of artificial microRNA transformed plants. Depicted is an agarose gel showing amplification of the artificial microRNA for different transformed plants with the 331 plasmid. Leaves from 5-week-old T2 generation plants were taken for DNA extraction using Thermo Fisher's Plant DNAzol reagent. Primers attB2R and att1BF were used to amplify the 200bp artificial microRNA. All plants transformed with the 331-plasmid showed amplification for the artificial microRNA. Positive control, (+), represents purified DNA of the pSES331 plasmid and negative control, (-), represents water used as template DNA.

2.2.3 *Analyzing stomatal development and gene expression of target genes*

In order to understand if downregulation of SBT 1.7 genes (Bradi1g07840 & Bradi1g14860) affects stomatal development *Brachypodium distachyon*, stomatal imaging and analysis was conducted (Figure 2.8). Stomatal index and density measurements was calculated using the 4th true leaf from three 5-week-old plants per insertion event (Figure 2.8 A & B). Stomatal density per area calculations in the azygous control, 331-1 and 322-1 plasmid containing plants showed no drastic impact to the number of stomata in the plasmid containing plants. (Figure 2.8.A). Similarly, stomatal index was calculated to determine if there was a difference in the number of stomata per pavement cell between the azygous control and the

plasmid-containing plants. In (Figure 2.8.B) stomatal index calculations showed no distinct change to the number of stomata in the plasmid containing plants with respect to the azygous control.

To investigate how effectively the artificial microRNA was downregulating the target genes (Bradi1g07840 & Bradi1g14860), gene expression analysis was conducted using real time quantitative PCR (Figure 2.9 & 2.10). After genotyping and confirming plants containing the artificial microRNA, RNA was extracted from healthy 5-week-old plants. Before cDNA was synthesized, samples were exposed to DNase to get rid of any potential DNA. Once cDNA was synthesized, real time quantitative PCR was conducted on a 96-well thermocycler using Syber green master mix. Real Time qPCR results conducted on 322-plasmid containing plants (Figure 2.9) show relatively weak downregulation of the target genes. Plant #1 and #3 seem to show a greater expression of the target genes compared to the azygous controls and plant #2 and #4. Gene expression analysis of 322-plasmid containing plants was conducted multiple times and showed similar weak downregulation of target genes.

The expression of the artificial microRNA in the 331-plasmid is driven by two 35S promoters, whereas the artificial microRNA in the 322-plasmid expression is driven by a maize ubiquitin promoter. This difference in promoter driven expression led us to conduct gene expression analysis on 331-plasmid containing plants to determine if and to what extent the artificial microRNA is downregulating the two target genes (Bradi1g07840 & Bradi1g14860). In (Figure 2.10) real Time qPCR results conducted on 3 different 331-plasmid containing plants showed downregulation of the target gene (Bradi1g14860) in plant #2 and #3. Also, one of the target genes (Bradi1g07840) seemed to be unaffected in both azygous control plants and in the plasmid-containing plants.

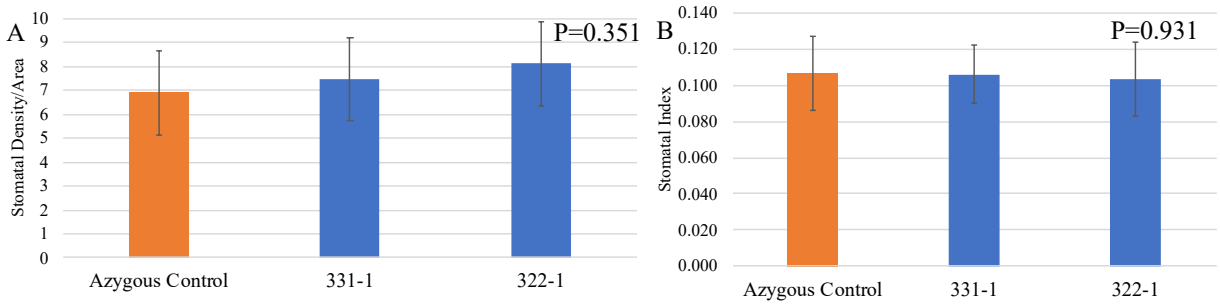

Figure 2.8. DIC leaf imaging of plasmid-containing 331-1 and 322-1 plants show similar stomatal development as azygous control. (A, B**)** DIC stomatal imaging and index/density calculations indicate that pSES 331-1 and pSES322-1 insertion event targeting two SBT 1.7 genes (Bradi1g07840 and Bradi1g14860) may have relatively the same number of stomata compared to Azygous control. Average stomatal index and density was calculated using 3 images for the center of the 4th leaf from three five-week-old plants per genotype (9 images total). Leaves were imaged at 40x magnification. Error bars shown represent the standard deviation of average (A) stomatal density and (B) stomatal index between leaves in a given plant line.

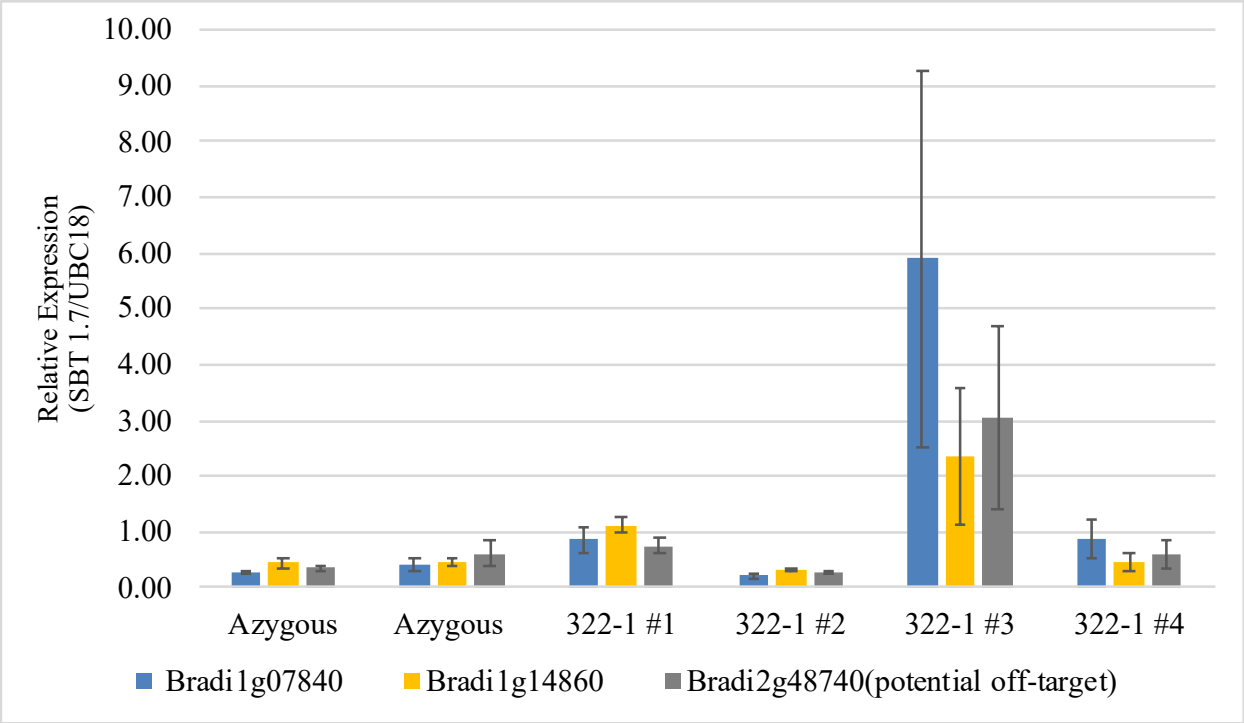

Figure 2.9.: Relative Gene Expression of amiRNA SBT 1.7 target genes. Shown are qPCR results of azygous controls and 322-1 plasmid-containing Brachypodium plants for the two target genes (Bradi1g07840 & Bradi1g14860) and a potential off-target(Bradi2g48740). Leaf tissue was collected from healthy 5-week-old plants and RNA was extracted using Spectrum Plant Total RNA Kit. cDNA was synthesized using a First-strand cDNA synthesis kit. The bar graphs represent 3 technical replicates per primer set. Data were normalized by the amount of housekeeping gene expressed, UBC 18.

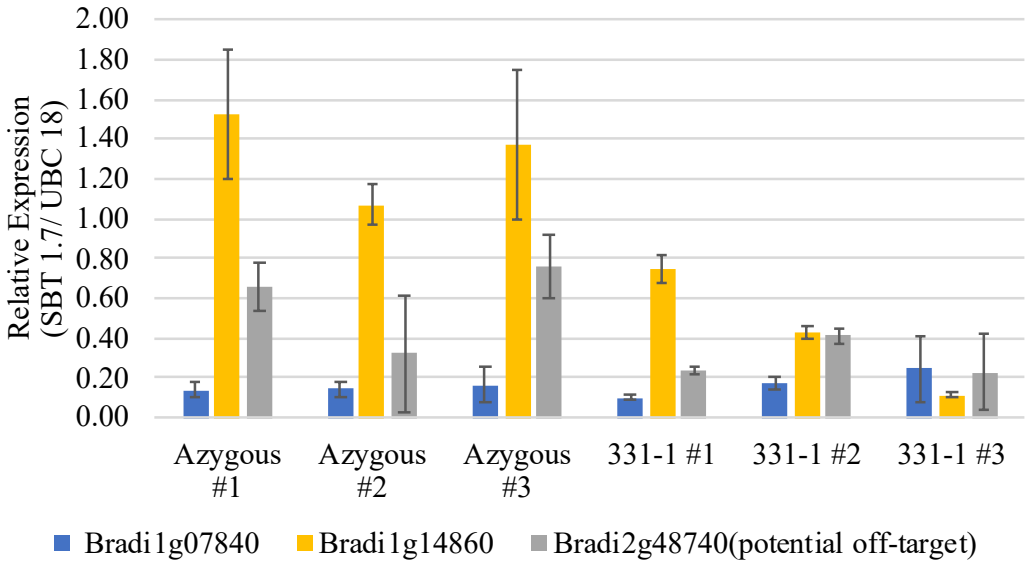

Figure 2.10: Relative Gene Expression of amiRNA SBT 1.7 target genes. Shown are qPCR results of azygous controls and 331-1 plasmid-containing Brachypodium plants for the two target genes (Bradi1g07840 & Bradi1g14860) and a potential off-target. Leaf tissue was collected from healthy 5-week-old plants and RNA was extracted using Spectrum Plant Total RNA Kit. cDNA was synthesized using First-strand cDNA synthesis kit. The bar graphs represent 3 technical replicates per primer set. Data were normalized by the amount of housekeeping gene expressed, UBC 18.

2.3 Discussion:

Our reverse genetic screen aimed at analyzing how silencing two SBT 1.7 genes (Bradi1g07840and Bradi1g14860) using designed artificial microRNAs would affect stomatal development in the grass model, *Brachypodium distachyon*. Our approach to select the target genes was based in part on the research done on stomatal development in *Arabidopsis Thaliana*. Stomatal development has been well studied in the dicot, *Arabidopsis thaliana*, compared to monocots. EPIDERMAL PATTERNING FACTOR (EPFs) are cysteine-rich signaling peptides that regulate stomatal development. Once cleaved and activated, EPF1 and EPF2 negatively regulate stomatal development, whereas when EPFL9/STOMAGEN is activated it positively regulates stomatal development (Richardson & Torii, 2013). In Arabidopsis, EPF2 has been

shown to be an important element for CO_2-dependent regulation of stomatal development (Engineer et al., 2014). One of the enzymes found to cleave and activate EPF2 in *Arababidopsis Thalinana* is a secreted protease known as CO2 RESPONSE SECRETED PROTEASE (CRSP) (Engineer et al., 2014). With an understanding of stomatal development regulation in *Arabidopsis thaliana*, we decided to silence potential subtilase proteases expressed in leaves of monocot, *Brachypodium distachyon* to investigate if there would be differences in stomatal development compared to control plants.

Since very little is known as to which subtilase proteases may play a role in regulating stomatal development in the monocot, *Brachypodium distachyon,* apoplastic proteomics was conducted on leaves. The apoplast is the space outside the plasma membrane and is known to play a role in various processes such as intercellular signaling, transport of water and nutrients (Sattelmacher et al., 2001) and has been shown to contain enzymes (L. Zhang et al., 2009). Our data showed SBT 1.7 genes to be highly expressed in leaves of *Brachypodium distachyon*. Moreover, artificial microRNA's have been shown to also downregulate homologs and since our approach to downregulate SBT 1.7 genes was to use this tool, a phylogenetic tree was generated to find potential off-target homologs that can be used to examine the specificity of the artificial microRNA. The best potential off target was the 3rd gene in the SBT 1.7 family (Bradi4g24790). However, after analyzing our transcriptomic data it was determined that the expression levels of this gene either at low (150ppm) or high (900ppm) was too low. This suggests that if the artificial microRNA did downregulate (Bradi4g24790), it would be challenging to measure any difference compared to the normal levels of expression. As a result, the next best homolog was chosen (Bradi2g48740).

Our approach to examine if subtilase enzymes in *Brachypodium distachyon* regulate stomatal development was to use artificial microRNA's. they have been used in plants to knockdown endogenous (Hauser et al., 2013; Ossowski et al., 2008)**,** including monocots. The downregulation of one or a set of genes results in a scorable phenotype. For example, *OsMIR390-AtL*-derived amiRNAs have been created to downregulate the target gene in *Brachypodium distachyon*, *BRASSINOSTEROID-INSENSITIVE 1* (*BdBRI1)* (Carbonell et al., 2015). Brassinosteroids are known to regulate many genes that play a role in overall plant development (Adam et al., 1999). Plants containing an artificial microRNA targeting *BRI1 driven* by a 35S promoter in *Brachypodium distachyon* were shorter in stature compared to the control plant and had bent out of shape leaves.

To determine if the artificial microRNA targeting the two SBT 1.7 genes (Bradi1g07840 & Bradi1g14860) would impact stomatal development and give us a scorable phenotype, we first began by conducting thermal imaging at ambient CO_2. If the two target genes did play a role in regulation of stomatal development, we would expect plasmid-containing plants have a difference in transpiration and, therefore, leaf temperature compared to control plants. Our thermal imaging data shows plasmid containing plants from either pSES322 or pSES331 with cooler or similar leaf temperature relative to the azygous control. This made it challenging to use thermal imaging as a scorable phenotype to identify plasmid-containing plants. Nonetheless, to avoid bias, genotyping would be conducted after thermal images were taken and only plants showing amplification for the artificial microRNA or resistance to hygromycin would be considered.

To investigate if the artificial microRNA targeting the two SBT 1.7 genes (Bradi1g07840 & Bradi1g14860) would impact stomatal development, stomatal imaging and analysis was

conducted. Our stomatal index and density calculations suggests that there is no significant difference between either the plasmid containing plants and the azygous control. This suggests that the artificial microRNA is not effectively downregulating the target genes and, as a result, differences in stomatal development between both groups is not observable. To examine this, gene expression analysis was conducted to determine the specificity of the artificial microRNA and to what extent it downregulated the target genes (Bradi1g07840 & radi1g14860). To do this, RNA was extracted from healthy 5-week-old and cDNA was synthesized. After conducting real time quantitative PCR, relative gene expression of all genes was calculated. Our gene expression results for plants containing the pSES322 plasmid indicate weak downregulation of the two target genes. Moreover, our gene expression results for plants containing the pSES331 plasmid show a downregulation of one of the target genes (Bradi1g14860), whereas the second target gene (Bradi1g07840) is the same for the azygous control and plasmid containing plants. Artificial microRNA's have been shown to successfully downregulate genes in *Brachypodium distachyon*. However, our gene expression analysis for pSES322 plasmid-containing plants show weak downregulation. This may be due to a feature in plants known as gene redundancy. Gene redundancy can prevent the plants expressing the artificial microRNA targeting the two SBT 1.7 genes from showing differences in stomatal development. It is conceivable that although the artificial microRNA downregulates the target genes, it is possible that genes similar in function play the same role. Therefore, if the redundant genes play the same role as the downregulated target genes, this would make it challenging to observe differences in stomatal development and leaf temperature phenotype. To continue pursuing the goal in this experiment, further experiments need to be conducted to examine if there are noticeable differences in expression levels of the SBT 1.7 enzymes. Furthermore, alternate approaches such as CRISPR/cas9-

mediated mutation in or deletion of these genes would be more effective than amiRNAs and could provide more robust information on the functions of the targeted SBT1.7 genes.

The human population is growing and can reach the limit of food crop-derived food production in light of climate change-dependent yield reductions. With the increase in pressure on food crop production, and the continuing increase in atmospheric CO_2, manipulation of stomatal development via peptide signaling in the grass model *Brachypodium distachyon* can provide answers that will inform scientists on how to improve crop production for the future.

2.4 Methods:

1. Generation of transgenic lines
2. Plant Material AmiRNA/ Growth conditions
3. DNA extraction and PCR-based genotyping:
4. Thermal imaging
5. DIC Imaging and Stomatal analysis
6. Real Time quantitative Polymerase Chain Reaction (RT-qPCR)
7. Hygromycin Resistance Screen protocol:

2.4.1 *Generation of transgenic lines:*

The amiRNA, 5' GAAGAACTCCACGGGCGTCCA 3' , was cloned into two vectors that have been used for amiRNA mediated gene-silencing in *Brachypodium* (Carbonell et al., 2015). Plasmid constructs pSES322 with rice and maize ubiquitin promoter and pSES331 with two 35S promoters were designed by Dr. Felix Hauser and cloned by Dr. Sebastian Schulze to knockdown Bradi1g07840 and Bradi1g14860 from the SBT 1.7 family in *Brachypodium distachyon*. Plasmids were submitted to the Boyce Thompson Institute Biotechnology Center for

AGL1 Agrobacterium transformation (Vogel & Hill, 2008). We obtained 4-5 independent insertion event T1 plants for each construct.

2.4.2 *Plant Material:*

Brachypodium distachyon plant lines of the Bd21-3 ecotype were used for investigating potential amiRNA downregulation of SBT 1.7 genes. Before potting, seeds were initially placed on plates and cold-treated for 7 days minimum at 4°C. In order to increase the water retention of the soil, a 1:1 ratio of vermiculite to perlite, was added to the soil. Individual germinated seeds for each genotype were potted in individual small pots. Light intensity in the growth room was set to 250 $\mu E\ m^{-2}\ s^{-1}$ to improve the growth conditions. Plants were exposed to an average atmospheric CO_2 of 450 ppm and a 16-hour light/8-hour dark cycle. To maintain a consistent level of soil moisture, plants are given a minimum of 1L of water with added fertilizer every other day.

2.4.3 *DNA extraction and PCR-based genotyping:*

Genomic DNA was extracted from plants for PCR-based genotyping by placing 1-2 leaves of each respective plant into 1.5 ml microcentrifuge tubes, containing a metal bead, and then dipped in liquid nitrogen. To crush leaf tissue, the tubes were placed in a grinder for 2 minutes at a speed of 25 cycles per second. Once the leaf tissue became powder form, the microcentrifuge tubes were placed back in liquid nitrogen. Following the Thermo Fisher Scientific Plant DNA extraction protocol (Waltham, Massachusetts 10978021), DNAzol reagent and the respective reagents were used to purify genomic DNA.

Primers attB2F and attB1R were used to amplify a 200 bp region of the pSES-322 and pSES-331 plasmid using Polymerase chain reaction (PCR). This region was used to determine whether or not the transformed plants contained the plasmid. For a positive control, the purified plasmids used to transform the plants were utilized and water was used as a negative control for DNA template.

2.4.4 *Thermal Imaging Analysis:*

Thermal imaging was conducted at ambient CO_2 on plants that are 5-6 weeks old using a FLIR Thermal Imaging camera T650sc (FLIR Systems, Inc. Wilsonville, OR 97070 USA). Ambient CO_2 thermal imaging took place in the growth room where the plants are grown. Azygous plants were used as control instead of WT, Bd21-3. Azygous plants and plasmid-containing plant lines were grown in parallel and under the same conditions.

2.4.5 *DIC Imaging and Stomatal analysis*

Stomatal imaging was conducted using an epidermal peel technique developed by Morgana Sidhom and myself. 5-6-week-old plants were used to determine stomatal density and index. First, we remove the 4^{th} true leaf and apply a small dot of glue (Loctite Super Glue) on a slide. We set the center of the leaf on the dot of glue and press down as evenly as possible to prevent formation of an air bubble. Once the glue has hardened, we gently peel off the leaf from the slide and image the impression on the slide using a Differential Interference Contrast (DIC) microscope with a camera. The image is taken at 40x magnification and four images are taken per slide. Stomatal pores and pavement cells were counted if fully contained within the image using the “cell-counter” tool from ImageJ.

2.4.6 *Real Time quantitative Polymerase Chain Reaction (RT-qPCR)*

In order to identify the best controls for conducting Real time quantitative PCR, I took the coding sequence of our target genes (Bradi1g14860 & Bradi1g07840) and used JGI's Phytozome tool BLAST to identify any homologs. After generating a phylogenetic tree, I was able to identify the best option for a potential off-target homolog to be the 3rd gene in the SBT 1.7 family (Bradi4g24790). Our transcriptomic data for Bradi4g24790 showed low expression levels in both high and low CO_2 making it challenging to identify any potential changes due to the artificial microRNA. As a result, I chose an alternative SBT gene, Bradi2g48740. In addition, to determine housekeeping gene controls, we found Bradi4g00660 (UBC18) and Bradi1g06851 (EF1α) to be the overall best (Hong et al., 2008).

RNA was extracted from azygous and plasmid-containing plants using the Spectrum Plant Total RNA kit (Sigma Aldrich). The quality of the RNA samples was analyzed using absorbance measurements from a nanodrop spectrophotometer. Before synthesizing cDNA, RNA samples were treated with a RNase-free DNase to get rid of any contaminating genomic DNA. Using GE's Healthcare First-strand synthesis kit, cDNA was synthesized according to protocol. Real time-qPCR runs were carried out in 96-well blocks using Bio-Rad CFX Connect Real-Time PCR Detection system, using SYBR Green PCR Master Mix. The thermal cycling reaction ran for 35-40 cycles that included at 95°C for 10 seconds, at 60°C for 30 seconds, and at 72°C for 30 seconds. All qRT-PCR reactions were carried out with 3 technical replicates.

The threshold cycle (Ct) values was calculate by averaging the three technical replicate values. The ΔΔCt method (Kozera & Rapacz, 2013) was used to calculate the relative gene

expression of the target genes in the azygous control and plasmid-containing plants relative to the housekeeping gene

2.4.7 *Hygromycin Resistance Screen protocol:*

The hygromycin resistance screen was used to genotype and identify plants containing either the pSES322 or pSES331 plasmid. Within the different components of the plasmids, an antibiotic resistance gene for hygromycin is included. Plants that do contain the plasmid can confer resistance resistance to hygromycin and in our approach these plants remain green after exposure to the antibiotic.

Agar plate preparation:

Materials: Included a 1,000mL glass storage bottle, 1,000mL graduated cylinder, 1,000mL plastic beaker, MES, MS + vitamins, Agar Phytozome, Hygromycin (50 ug/mL)

, 12X12 cm square petri dish plates, and KOH. (this recipe will be enough to prepare about 12 agar plates)

1. Measure 800 mL of milliQ water using a graduated cylinder and pour into the 1,000 mL plastic beaker.
2. Weigh out 1.76 g of MS + vitamins and pour in plastic beaker
3. Weigh out 0.40 g of MES and pour in plastic beaker
4. Place plastic beaker on stirrer, insert a stir bar and pH bar to determine how much base is needed to reach a pH of 5.8. Since we are working with plants, only use KOH to increase the pH instead of NaOH as it can be toxic to plants.
5. Once the pH 5.8 is achieved, grab the 1,000 mL glass storage bottle and measure out 6.40 g of Phyto Agar.

6. Add the Phyto Agar to the glass bottle and then transfer the contents from the plastic beaker into the glass bottle.
7. Next, autoclave the 1,000 mL glass storage bottle.
8. Once the bottle and the contents inside are autoclaved, let the bottle cool down to room temperature, and then add 0.64 mL of [50 ug/mL] Hygromycin to an 800mL agar solution. Once this is done, the solution is ready to be poured.
9. When pouring the mixture on the plates, pour them a little thicker than normally done for seeds. Next, to store the Hygromycin-containing agar plates, tape them with two layers of micropore tape and place them in a refrigerator or cold-room.

Transferring leaves onto agar plate:

Note: Use Brachypodium plants that are about 5 weeks old and take the tips of leaves that are completely expanded. Before you begin cutting the tips off the plant leaves, determine how many you will use and then use a permanent marker to outline and divide the 12X12cm square agar plate into individual boxes.

1. Take a 12x12cm hygromycin-containing agar plate, unwrap it and place the lid to the side.
2. Using mini scissors, cut the tips off leaves that are completely expanded from the transgenic plants you plan to use in the Resistance Screen.
3. Using forceps, place the cut tips into the hygromycin-containing agar plate at an angle and ensure that the abaxial side of all the cut leaves is facing down when inside the plate.
4. Once all the plants are snipped and the tips are placed in the selective media, put the lid back on and tape with two layers of micropore tape.

5. Place all the prepared plates in a growth chamber or where your specified plants are typically grown and place the plates horizontally.
6. Typically, you will begin to see results after 3 days and the clearest results occur around 5 days. (note: the leaves that are resistant to hygromycin will stay green, whereas the susceptible ones will turn white at the tips or darken in the middle of the leaf.)

References:

Adam, G., Schmidt, J., & Schneider, B. (1999). Brassinosteroids. In *Fortschritte der Chemie organischer Naturstoffe. Progress in the chemistry of organic natural products. Progrès dans la chimie des substances organiques naturelles*. https://doi.org/10.1201/9781439821831.ch13

Assmann, S. M., & Jegla, T. (2016). Guard cell sensory systems: recent insights on stomatal responses to light, abscisic acid, and CO2. In *Current Opinion in Plant Biology*. https://doi.org/10.1016/j.pbi.2016.07.003

Bartel, D. P. (2004). MicroRNAs: Genomics, Biogenesis, Mechanism, and Function. In *Cell*. https://doi.org/10.1016/S0092-8674(04)00045-5

Berger, D., & Altmann, T. (2000). A subtilisin-like serine protease involved in the regulation of stomatal density and distribution in Arabidopsis thaliana. *Genes and Development*. https://doi.org/10.1101/gad.14.9.1119

Bergmann, D. C., Lukowitz, W., & Somerville, C. R. (2004). Stomatal development and pattern controlled by a MAPKK kinase. *Science*. https://doi.org/10.1126/science.1096014

Bergmann, D. C., & Sack, F. D. (2007). Stomatal Development. *Annual Review of Plant Biology*. https://doi.org/10.1146/annurev.arplant.58.032806.104023

Bologna, N. G., & Voinnet, O. (2014). The Diversity, Biogenesis, and Activities of Endogenous Silencing Small RNAs in Arabidopsis . *Annual Review of Plant Biology*. https://doi.org/10.1146/annurev-arplant-050213-035728

Brandt, B., Brodsky, D. E., Xue, S., Negi, J., Iba, K., Kangasjärvi, J., Ghassemian, M., Stephan, A. B., Hu, H., & Schroeder, J. I. (2012). Reconstitution of abscisic acid activation of SLAC1 anion channel by CPK6 and OST1 kinases and branched ABI1 PP2C phosphatase action. *Proceedings of the National Academy of Sciences of the United States of America*. https://doi.org/10.1073/pnas.1116590109

Brkljacic, J., Grotewold, E., Scholl, R., Mockler, T., Garvin, D. F., Vain, P., Brutnell, T., Sibout, R., Bevan, M., Budak, H., Caicedo, A. L., Gao, C., Gu, Y., Hazen, S. P., Holt, B. F., Hong, S. Y., Jordan, M., Manzaneda, A. J., Mitchell-Olds, T., Mochida, K., Mur, L. A. J., Park, C. M., Sedbrook, J., Watt, M., Zheng, S. J., & Vogel, J. P. (2011). Brachypodium as a model for the grasses: Today and the future. *Plant Physiology*. https://doi.org/10.1104/pp.111.179531

Brodribb, T. J., Sussmilch, F., & McAdam, S. A. M. (2019). From reproduction to production, stomata are the master regulators. *Plant Journal*. https://doi.org/10.1111/tpj.14561

Cai, S., Papanatsiou, M., Blatt, M. R., & Chen, Z. H. (2017). Speedy Grass Stomata: Emerging Molecular and Evolutionary Features. In *Molecular Plant* (Vol. 10, Issue 7, pp. 912–914). Cell Press. https://doi.org/10.1016/j.molp.2017.06.002

Carbonell, A., Fahlgren, N., Mitchell, S., Cox, K. L., Reilly, K. C., Mockler, T. C., & Carrington, J. C. (2015). Highly specific gene silencing in a monocot species by artificial microRNAs derived from chimeric miRNA precursors. *Plant Journal*. https://doi.org/10.1111/tpj.12835

Casson, S. A., & Hetherington, A. M. (2010). Environmental regulation of stomatal development. In *Current Opinion in Plant Biology*. https://doi.org/10.1016/j.pbi.2009.08.005

Ceciliato, P. H. O., Zhang, J., Liu, Q., Shen, X., Hu, H., Liu, C., Schäffner, A. R., & Schroeder, J. I. (2019). Intact leaf gas exchange provides a robust method for measuring the kinetics of stomatal conductance responses to abscisic acid and other small molecules in Arabidopsis and grasses. *Plant Methods*. https://doi.org/10.1186/s13007-019-0423-y

Cominelli, E., Galbiati, M., Vavasseur, A., Conti, L., Sala, T., Vuylsteke, M., Leonhardt, N., Dellaporta, S. L., & Tonelli, C. (2005). A guard-cell-specific MYB transcription factor regulates stomatal movements and plant drought tolerance. *Current Biology*. https://doi.org/10.1016/j.cub.2005.05.048

Draper, J., Mur, L. A. J., Jenkins, G., Ghosh-Biswas, G. C., Bablak, P., Hasterok, R., & Routledge, A. P. M. (2001). Brachypodium distachyon. A new model system for functional genomics in grasses. *Plant Physiology*. https://doi.org/10.1104/pp.010196

Engineer, C. B., Ghassemian, M., Anderson, J. C., Peck, S. C., Hu, H., & Schroeder, J. I. (2014). Carbonic anhydrases, EPF2 and a novel protease mediate CO2 control of stomatal development. *Nature*. https://doi.org/10.1038/nature13452

Engineer, C. B., Hashimoto-Sugimoto, M., Negi, J., Israelsson-Nordström, M., Azoulay-Shemer, T., Rappel, W. J., Iba, K., & Schroeder, J. I. (2016). CO2 Sensing and CO2 Regulation of Stomatal Conductance: Advances and Open Questions. In *Trends in Plant Science* (Vol. 21, Issue 1). https://doi.org/10.1016/j.tplants.2015.08.014

Geiger, D., Scherzer, S., Mumm, P., Stange, A., Marten, I., Bauer, H., Ache, P., Matschi, S., Liese, A., Al-Rasheid, K. A. S., Romeis, T., & Hedrich, R. (2009). Activity of guard cell anion channel SLAC1 is controlled by drought-stress signaling kinase-phosphatase pair. *Proceedings of the National Academy of Sciences of the United States of America*. https://doi.org/10.1073/pnas.0912021106

Geisler, M., Nadeau, J., & Sack, F. D. (2000). Oriented asymmetric divisions that generate the stomatal spacing pattern in Arabidopsis are disrupted by the too many mouths mutation. *Plant Cell*. https://doi.org/10.1105/tpc.12.11.2075

Hashimoto, M., Negi, J., Young, J., Israelsson, M., Schroeder, J. I., & Iba, K. (2006). Arabidopsis HT1 kinase controls stomatal movements in response to CO2. *Nature Cell Biology*. https://doi.org/10.1038/ncb1387

Hauser, F., Chen, W., Deinlein, U., Chang, K., Ossowski, S., Fitz, J., Hannon, G. J., & Schroeder, J. I. (2013). A genomic-scale artificial MicroRNA library as a tool to investigate the functionally redundant gene space in arabidopsis. *Plant Cell*. https://doi.org/10.1105/tpc.113.112805

Hepworth, C., Caine, R. S., Harrison, E. L., Sloan, J., & Gray, J. E. (2018). Stomatal development: focusing on the grasses. In *Current Opinion in Plant Biology* (Vol. 41). https://doi.org/10.1016/j.pbi.2017.07.009

Hetherington, A. M., & Woodward, F. I. (2003). The role of stomata in sensing and driving environmental change. In *Nature*. https://doi.org/10.1038/nature01843

Hong, S. Y., Seo, P. J., Yang, M. S., Xiang, F., & Park, C. M. (2008). Exploring valid reference genes for gene expression studies in Brachypodium distachyon by real-time PCR. *BMC Plant Biology*. https://doi.org/10.1186/1471-2229-8-112

Hu, H., Boisson-Dernier, A., Israelsson-Nordström, M., Böhmer, M., Xue, S., Ries, A., Godoski, J., Kuhn, J. M., & Schroeder, J. I. (2010). Carbonic anhydrases are upstream regulators of CO2-controlled stomatal movements in guard cells. *Nature Cell Biology*. https://doi.org/10.1038/ncb2009

Jung, K. H., An, G., & Ronald, P. C. (2008). Towards a better bowl of rice: Assigning function to tens of thousands of rice genes. In *Nature Reviews Genetics*. https://doi.org/10.1038/nrg2286

Kanaoka, M. M., Pillitteri, L. J., Fujii, H., Yoshida, Y., Bogenschutz, N. L., Takabayashi, J., Zhu, J. K., & Torii, K. U. (2008). SCREAM/ICE1 and SCREAM2 specify three cell-state transitional steps leading to Arabidopsis stomatal differentiation. *Plant Cell*. https://doi.org/10.1105/tpc.108.060848

Kosma, D. K., & Jenks, M. A. (2007). Eco-physiological and molecular-genetic determinants of plant cuticle function in drought and salt stress tolerance. In *Advances in Molecular Breeding Toward Drought and Salt Tolerant Crops* (pp. 91–120). Springer Netherlands. https://doi.org/10.1007/978-1-4020-5578-2_5

Kozera, B., & Rapacz, M. (2013). Reference genes in real-time PCR. In *Journal of Applied Genetics*. https://doi.org/10.1007/s13353-013-0173-x

Kusumi, K., Hirotsuka, S., Kumamaru, T., & Iba, K. (2012). Increased leaf photosynthesis caused by elevated stomatal conductance in a rice mutant deficient in SLAC1, a guard cell anion channel protein. *Journal of Experimental Botany*. https://doi.org/10.1093/jxb/ers216

Lampard, G. R., Lukowitz, W., Ellis, B. E., & Bergmann, D. C. (2009). Novel and expanded roles for MAPK signaling in Arabidopsis Stomatal cell fate revealed by cell type-specific manipulations. *Plant Cell*. https://doi.org/10.1105/tpc.109.070110

Lampard, G. R., MacAlister, C. A., & Bergmann, D. C. (2008). Arabidopsis stomatal initiation is controlled by MAPK-mediated regulation of the bHLH SPEECHLESS. *Science*. https://doi.org/10.1126/science.1162263

Lau, O. S., & Bergmann, D. C. (2012). Stomatal development: A plant's perspective on cell polarity, cell fate transitions and intercellular communication. *Development (Cambridge)*. https://doi.org/10.1242/dev.080523

Lee, S. C., Lan, W., Buchanan, B. B., & Luan, S. (2009). A protein kinase-phosphatase pair interacts with an ion channel to regulate ABA signaling in plant guard cells. *Proceedings of the National Academy of Sciences of the United States of America*. https://doi.org/10.1073/pnas.0910601106

Macalister, C. A., & Bergmann, D. C. (2011). Sequence and function of basic helix-loop-helix proteins required for stomatal development in Arabidopsis are deeply conserved in land plants. *Evolution and Development*. https://doi.org/10.1111/j.1525-142X.2011.00468.x

McAinsh, M. R., & Taylor, J. E. (2016). Stomata. In *Encyclopedia of Applied Plant Sciences* (Vol. 1, pp. 128–134). Elsevier Inc. https://doi.org/10.1016/B978-0-12-394807-6.00073-3

McKown, K. H., & Bergmann, D. C. (2020). Stomatal development in the grasses: lessons from models and crops (and crop models). *New Phytologist*. https://doi.org/10.1111/nph.16450

Merlot, S., Mustilli, A. C., Genty, B., North, H., Lefebvre, V., Sotta, B., Vavasseur, A., & Giraudat, J. (2002). Use of infrared thermal imaging to isolate Arabidopsis mutants defective in stomatal regulation. *Plant Journal*. https://doi.org/10.1046/j.1365-313X.2002.01322.x

Muir, C. D. (2015). Making pore choices: Repeated regime shifts in Stomatal ratio. *Proceedings of the Royal Society B: Biological Sciences*. https://doi.org/10.1098/rspb.2015.1498

Munemasa, S., Hauser, F., Park, J., Waadt, R., Brandt, B., & Schroeder, J. I. (2015). Mechanisms of abscisic acid-mediated control of stomatal aperture. In *Current Opinion in Plant Biology*. https://doi.org/10.1016/j.pbi.2015.10.010

Mustilli, A. C., Merlot, S., Vavasseur, A., Fenzi, F., & Giraudat, J. (2002). Arabidopsis OST1 protein kinase mediates the regulation of stomatal aperture by abscisic acid and acts upstream of reactive oxygen species production. *Plant Cell*. https://doi.org/10.1105/tpc.007906

Negi, J., Hashimoto-Sugimoto, M., Kusumi, K., & Iba, K. (2014). New approaches to the biology of stomatal guard cells. In *Plant and Cell Physiology*. https://doi.org/10.1093/pcp/pct145

Negi, J., Matsuda, O., Nagasawa, T., Oba, Y., Takahashi, H., Kawai-Yamada, M., Uchimiya, H., Hashimoto, M., & Iba, K. (2008). CO2 regulator SLAC1 and its homologues are essential for anion homeostasis in plant cells. *Nature*. https://doi.org/10.1038/nature06720

Ossowski, S., Schwab, R., & Weigel, D. (2008). Gene silencing in plants using artificial microRNAs and other small RNAs. In *Plant Journal*. https://doi.org/10.1111/j.1365-313X.2007.03328.x

Pei, Z. M., & Kuchitsu, K. (2005). Early ABA signaling events in guard cells. In *Journal of Plant Growth Regulation*. https://doi.org/10.1007/s00344-005-0095-x

Pei, Z. M., Kuchitsu, K., Ward, J. M., Schwarz, M., & Schroeder, J. I. (1997). Differential abscisic acid regulation of guard cell slow anion channels in arabidopsis wild-type and abi1 and abi2 mutants. *Plant Cell*. https://doi.org/10.1105/tpc.9.3.409

Raissig, M. T., Matos, J. L., Gil, M. X. A., Kornfeld, A., Bettadapur, A., Abrash, E., Allison, H. R., Badgley, G., Vogel, J. P., Berry, J. A., & Bergmann, D. C. (2017). Mobile MUTE specifies subsidiary cells to build physiologically improved grass stomata. *Science*. https://doi.org/10.1126/science.aal3254

Reddy, A. R., Rasineni, G. K., & Raghavendra, A. S. (2010). The impact of global elevated CO2 concentration on photosynthesis and plant productivity. In *Current Science* (Vol. 99, Issue 1, pp. 46–57).

Richardson, L. G. L., & Torii, K. U. (2013). Take a deep breath: Peptide signalling in stomatal patterning and differentiation. In *Journal of Experimental Botany*. https://doi.org/10.1093/jxb/ert246

Roelfsema, M. R. G., Hanstein, S., Felle, H. H., & Hedrich, R. (2002). CO2 provides an intermediate link in the red light response of guard cells. *Plant Journal*, *32*(1), 65–75. https://doi.org/10.1046/j.1365-313X.2002.01403.x

Sattelmacher, B. (2001). The apoplast and its significance for plant mineral nutrition. In *New Phytologist* (Vol. 149, Issue 2, pp. 167–192). https://doi.org/10.1046/j.1469-8137.2001.00034.x

Scripps Institution of Oceanography. (2018). *The Keeling Curve*. UC San Diego. https://scripps.ucsd.edu/programs/keelingcurve/

Vahisalu, T., Kollist, H., Wang, Y. F., Nishimura, N., Chan, W. Y., Valerio, G., Lamminmäki, A., Brosché, M., Moldau, H., Desikan, R., Schroeder, J. I., & Kangasjärvi, J. (2008). SLAC1 is required for plant guard cell S-type anion channel function in stomatal signalling. *Nature*, *452*(7186), 487–491. https://doi.org/10.1038/nature06608

Vogel, J., & Hill, T. (2008). High-efficiency Agrobacterium-mediated transformation of Brachypodium distachyon inbred line Bd21-3. *Plant Cell Reports*. https://doi.org/10.1007/s00299-007-0472-y

Von Groll, U., Berger, D., & Altmann, T. (2002). The subtilisin-like serine protease SDD1 mediates cell-to-cell signaling during arabidopsis stomatal development. *Plant Cell*. https://doi.org/10.1105/tpc.001016

Woods, D. P., Ream, T. S., Bouché, F., Lee, J., Thrower, N., Wilkerson, C., & Amasino, R. M. (2017). Establishment of a vernalization requirement in Brachypodium distachyon requires REPRESSOR OF VERNALIZATION1. *Proceedings of the National Academy of Sciences of the United States of America*. https://doi.org/10.1073/pnas.1700536114

Xia, Z., Watanabe, S., Yamada, T., Tsubokura, Y., Nakashima, H., Zhai, H., Anai, T., Sato, S., Yamazaki, T., Lü, S., Wu, H., Tabata, S., & Harada, K. (2012). Positional cloning and characterization reveal the molecular basis for soybean maturity locus E1 that regulates photoperiodic flowering. *Proceedings of the National Academy of Sciences of the United States of America*. https://doi.org/10.1073/pnas.1117982109

Xue, S., Hu, H., Ries, A., Merilo, E., Kollist, H., & Schroeder, J. I. (2011). Central functions of bicarbonate in S-type anion channel activation and OST1 protein kinase in CO2 signal transduction in guard cell. *EMBO Journal*. https://doi.org/10.1038/emboj.2011.68

Zhang, J., Wang, N., Miao, Y., Hauser, F., McCammon, J. A., Rappel, W.-J., & Schroeder, J. I. (2018). Identification of SLAC1 anion channel residues required for CO2/bicarbonate sensing and regulation of stomatal movements. *Proceedings of the National Academy of Sciences*, *115*(44), 11129–11137. https://doi.org/10.1073/PNAS.1807624115

Zhang, L., Tian, L. H., Zhao, J. F., Song, Y., Zhang, C. J., & Guo, Y. (2009). Identification of an apoplastic protein involved in the initial phase of salt stress response in rice root by two-dimensional electrophoresis. *Plant Physiology*. https://doi.org/10.1104/pp.108.131144

Zoulias, N., Harrison, E. L., Casson, S. A., & Gray, J. E. (2018). Molecular control of stomatal development. In *Biochemical Journal* (Vol. 475, Issue 2). https://doi.org/10.1042/BCJ20170413